Boosting the host immune system to fight tuberculosis

Boland, R.

4

Repurposing Tamoxifen as potential host-directed therapeutic for tuberculosis

Ralf Boland[1*], Matthias T. Heemskerk[2*], Gabriel Forn-Cuní[1], Cornelis J. Korbee[2], Kimberley V. Walburg[2], Jeroen J. Esselink[2], Carina Carvalho dos Santos[2,3], Amy de Waal[1], Daniel C.M. van der Hoeven[1], Elisa van der Sar[1], Herman P. Spaink[1], Michiel van der Vaart[1], Annemarie H. Meijer[1#], Tom H. M. Ottenhoff[2#]

1. Institute of Biology Leiden, Leiden University, Leiden, The Netherlands
2. Department of Infectious Diseases, Leiden University Medical Center, Leiden, The Netherlands
3. Laboratório Especial de Desenvolvimento de Vacinas, Instituto Butantan, São Paulo, Brazil

*# Equal contribution

Manuscript under revision

Abstract

The global burden of Tuberculosis (TB) is aggravated by the continuously increasing emergence of drug resistance, urging for innovative therapeutic options. The concept of host-directed therapy (HDT) as adjunctive to classical antibacterial therapy with antibiotics represents a novel and promising approach for treating TB. Here, we have focused on repurposing the clinically used anti-cancer drug Tamoxifen, which was identified as a molecule with strong host-directed activity against intracellular *Mycobacterium tuberculosis* (*Mtb*). Using a primary human macrophage *Mtb* infection model, we demonstrate the potential of Tamoxifen against drug sensitive as well as drug resistant *Mtb* bacteria. The therapeutic effect of Tamoxifen was confirmed in an *in vivo* TB model, based on *Mycobacterium marinum* infection of zebrafish larvae. Tamoxifen had no direct antimicrobial effects at the concentrations used, confirming that Tamoxifen acted as a HDT drug. Furthermore, we demonstrate that the anti-mycobacterial effect of Tamoxifen is independent of its well-known target, the estrogen receptor (ER) pathway, but instead acts by modulating autophagy and in particular the lysosomal pathway. Through RNA sequencing and microscopic colocalization studies, we show that Tamoxifen stimulates lysosomal activation and increases the localization of mycobacteria in lysosomes both *in vitro* and *in vivo*. Thus, our work highlights the HDT potential of Tamoxifen and proposes it as a repurposed molecule for the treatment of TB.

Introduction

It is estimated that 1.7 billion people are latently infected with *Mycobacterium tuberculosis (Mtb*), the infectious agent causing tuberculosis (TB)[1]. In 2020, there were 10 million new cases and 1.4 million people died from the disease[2]. There is an alarming contribution of multidrug-resistant (MDR-TB) and extensively drug-resistant (XDR-TB) infections to the global antimicrobial resistance (AMR) disease burden[2]. Currently, there is no effective TB vaccine available, and the only licensed vaccine in use, Bacille Calmette-Guérin (BCG) has limited protective efficacy[3]. Although in the last decade a few new antibiotics have been approved for the treatment of MDR and XDR TB, including Bedaquiline[4], Delamanid[5], Linezolid[6] and Pretomanid[7], mutations conferring resistance against these drugs have already been found[8]. Therefore, novel tools and strategies are needed to combat this global threat, including more effective therapeutics that shorten the prolonged regimens of TB treatment (currently 6 months or more) and help preventing *de novo* resistance and TB relapse.

Intracellular bacteria such as *Mtb* manipulate cellular signaling pathways to promote their own survival in human cells, by creating a replicative niche or by subverting the immune system[9,10]. As a complement to classical antibiotics, host-directed therapy (HDT) has recently emerged as a novel concept in TB: HDT aims to enhance host defense by modulating processes in the host that restrict growth and survival of bacteria in their intracellular niches[11-15]. Large-scale chemical and genetic screens of molecular libraries targeting *Mtb*-infected cells have revealed a variety of potential HDT candidates that could be repurposed to combat TB, including groups of anti-inflammatory drugs, anti-psychotic drugs, and kinase inhibitors. These compounds affecting inflammatory pathways, lipid metabolism, and autophagy could be effective against both antibiotic-sensitive and -resistant bacteria, including MDR and XDR TB[11-15].

Autophagy is an intracellular degradation pathway vital to maintaining homeostasis by removing unwanted elements from the cytosol, such as misfolded protein aggregates, damaged organelles, and microbial invaders[16]. Due to the pro-homeostatic function of autophagy, drugs that modulate this process are currently being investigated as novel therapeutics for a wide variety of diseases[17]. Autophagy can inhibit intracellular infection by promoting the delivery of pathogens to lysosomes[18]. Although virulence mechanisms of pathogens may counteract autophagy to some extent, several studies have shown that induction of autophagy restricts *Mtb* intracellular growth and promotes its lysosomal degradation[16,19,20]. For these reasons, autophagy has become a priority target for anti-(myco)bacterial HDT development[13,15,18,21].

Tamoxifen, widely known for its use as a breast-cancer therapeutic[22-24], was identified as a promising molecule for host-directed inhibition of intracellular *Mtb* when we previously screened an autophagy-modulating compound library *in vitro* in human cells[25]. The main known targets of Tamoxifen are estrogen receptors (ERs). Tamoxifen can function either as an agonist or antagonist of the ER, depending on the presence of co-regulatory transcription factors[23]. Besides its use in breast-cancer therapy, Tamoxifen has more recently been studied in the context of various microbial infections and was found to possess direct antimicrobial effects against *Cryptococcus* and *Leishmania*[26,27]. In addition, it was reported that Tamoxifen had a direct anti-bacterial effect on *Mtb*, synergizing with first-line TB-antibiotics[28,29]. In contrast to these reported direct anti-microbial effects, there is evidence that the inhibitory effect of Tamoxifen on intracellular *Toxoplasma* growth is mediated in a host-directed manner by inducing autophagic degradation of the parasite-containing vacuole[30]. However, the role of Tamoxifen-induced autophagy and possibly other Tamoxifen-modulated host pathways in controlling *Mtb* or other bacterial infections remains incompletely defined.

In this study we have used *in vitro* and *in vivo* TB models to investigate the anti-bacterial and host-directed effects of Tamoxifen, and to elucidate the potential host-directed mechanisms involved. Lung-resident macrophages, consisting mainly of alveolar macrophages, represent the predominant host cell in the initial stages of *Mtb* infection[31,32]. The different functional responses of these cells can be represented by differentiating primary human macrophages *in vitro* into pro- and anti-inflammatory polarization states[33], which proved an effective approach to explore drug efficacy[34-36]. To investigate the *in vivo* therapeutic potential of Tamoxifen, we used the zebrafish TB model, which reiterates many features of human TB pathogenesis[37-39]. Specifically, the infection of zebrafish embryos with *Mycobacterium marinum* (*Mm*), which shares major virulence factors with *Mtb*, results in the development of granulomatous aggregates of leukocytes, the hallmark pathology of TB. Moreover, we have previously demonstrated that autophagy is a critical host defense mechanism of zebrafish to *Mm* infection, which makes this model well suited to investigate the autophagy-modulating properties of Tamoxifen in relation to mycobacterial pathogenesis[40-43].

Using *in vitro* infected human macrophages, we demonstrate a clear HDT effect of Tamoxifen against both drug-susceptible and MDR-*Mtb* strains. Furthermore, we found that Tamoxifen's HDT effect against intracellular mycobacteria is independent of ER signaling, both *in vitro* and *in vivo*. Complementary transcriptome profiling of zebrafish larvae revealed significant effects of Tamoxifen on pathways related to autophagy and lysosomal processes, both in the absence and presence of infection. Colocalization analyses of *Mtb* and *Mm* with autophagosomal and lysosomal markers showed that the HDT effect of Tamoxifen could not be directly attributed to its autophagy-inducing properties, but appears linked to modulation of lysosomal function and increased

delivery of mycobacteria to lysosomes. In conclusion, our results suggest that Tamoxifen inhibits intracellular mycobacteria primarily by promoting the efficacy of the lysosomal pathway, which was cross-validated across different hosts and different mycobacterial pathogens. Our findings position this clinically approved drug as a strong candidate for repurposing as an HDT molecule against TB, especially MDR- and XDR-TB.

Results

In vitro identification of Tamoxifen as a novel repurposed host-directed therapeutic

For *de novo* discovery of drugs with potential activity against intracellular *Mtb* we previously screened the Screen-Well Autophagy Library of clinically approved molecules, which identified Tamoxifen as a promising candidate[25]. To validate this initial screening result we tested Tamoxifen in our previously described primary human macrophage model system: we compared Tamoxifen's effects on intracellular infection in two polarized macrophage subsets, pro-inflammatory (Mφ1) and anti-inflammatory (Mφ2) macrophages[34,44,45]. Classical colony forming unit assays (CFU) were used to measure the effect of 24-hour treatment on *Mtb*-infection (Figure 1A). Tamoxifen treatment showed a significant decrease of *Mtb* outgrowth in both Mφ1 and Mφ2 (median reduction of detectable bacteria of 29% and 44%, respectively). To test whether Tamoxifen could also target another intracellular pathogen, we infected Mφ1 and Mφ2 with *Salmonella enterica* serovar Typhimurium (*Stm*) (Figure 1B). Tamoxifen showed high efficacy against intracellular *Stm* outgrowth (in several donors we observed up to 99% reduction of detectable bacteria).

To confirm that Tamoxifen acts in a host-directed and not direct antibacterial manner, we treated both *Mtb* and *Stm* in liquid broth with Tamoxifen at the same concentration (10 μM). *Mtb* growth was unaffected by the presence of Tamoxifen compared to negative control solvent DMSO, whereas the positive control anti-*Mtb* antibiotic rifampicin inhibited *Mtb* growth as expected (Figure 1C). Similarly, 10 μM of Tamoxifen

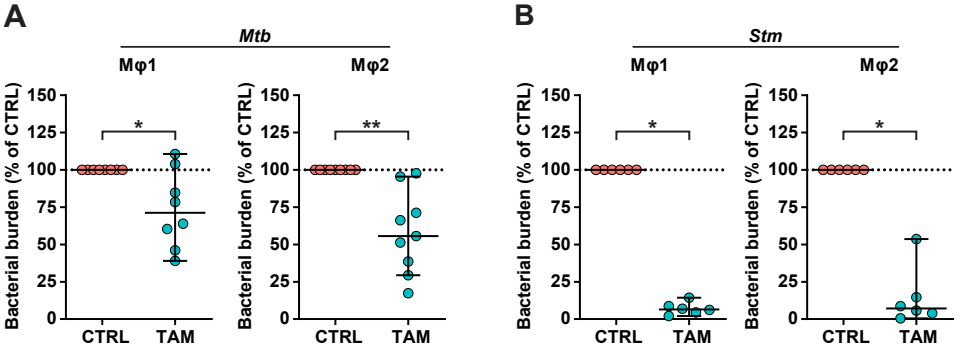

Figure 1. *In vitro* identification of Tamoxifen as a novel repurposed host-directed therapeutic

A-B. CFU assay of Mφ1 (left) and Mφ2 (right) infected with H37Rv-*Mtb* (A) or *Stm* (B) and treated with 10 μM of Tamoxifen or control (DMSO at equal v/v) for 24 hours. Each dot represents a single donor (8 and 9 donors for Mφ1 and Mφ2 respectively in A and 6 donors in B) and depicts the mean of 3 or 4 replicates. Dotted lines indicate control set at 100% and median + 95% confidence intervals are shown for every condition. Statistical significance was tested using Wilcoxon matched-pairs signed rank test.

Figure and figure legend continued on next page.

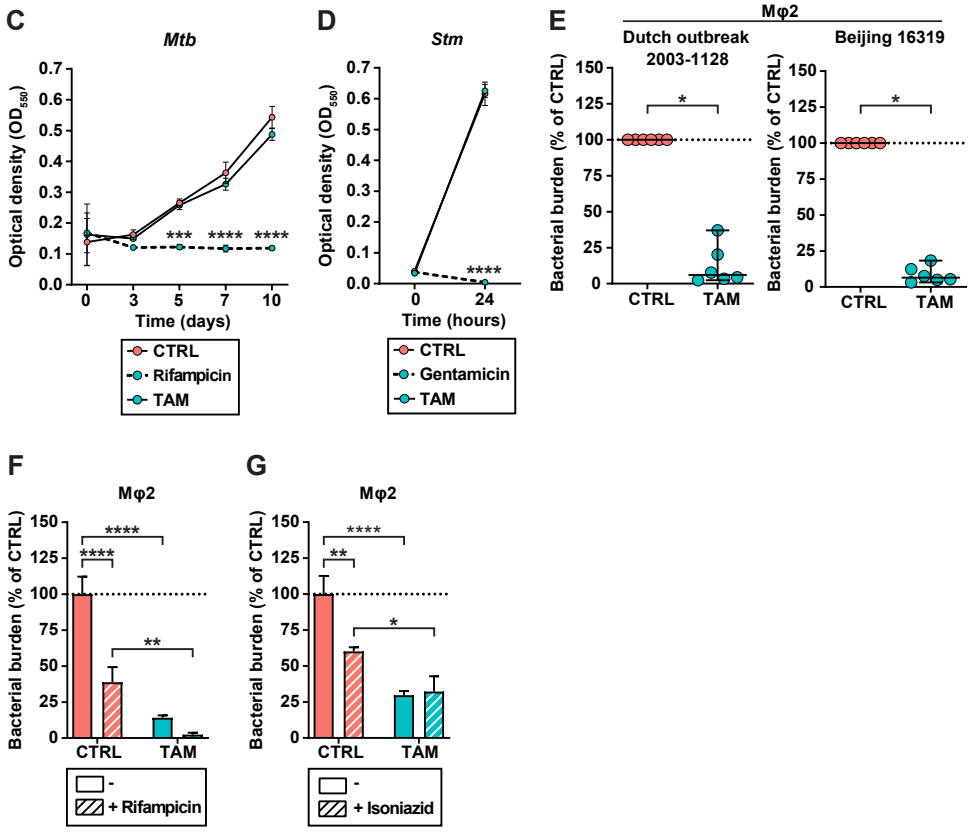

Figure 1. (continued)

C-D. H37Rv-*Mtb* growth (C) or *Stm* growth (D) in liquid culture during treatment with 10 μM of Tamoxifen or control (DMSO at equal v/v) up to assay endpoint, day 10 (C) or overnight (D). Rifampicin (20 μg/ml) (C) or Gentamicin (50 μg/ml) (D) was used as a positive control for growth inhibition. Each line depicts the mean ± standard deviation of 3 replicates. Experiment shown is a representative of 3 independent experiments. Statistical significance of treatment versus control treatment was tested using a two-way ANOVA with Dunnett's multiple comparisons test.

E. CFU assay of Mφ2 infected with MDR-*Mtb* strain Dutch outbreak 2003-1128 (left panel) or *Mtb* Beijing strain 16319 (right panel) and treated with 10 μM of Tamoxifen or control (DMSO at equal v/v) for 24 hours. Each dot represents a single donor (6 donors in total) and depicts the mean of 3 replicates. Dotted lines indicate control treatment set at 100% and median + 95% confidence intervals are shown for every condition. Statistical significance was tested using Wilcoxon matched-pairs signed rank test.

F-G. CFU assay of Mφ2 infected with H37Rv-*Mtb* and treated for 24 hours with 10 μM of Tamoxifen or control (DMSO at equal v/v) in combination with suboptimal doses of the antibiotics Rifampicin (F, 0.05μg/ml) or Isoniazid (G, 0.4 μg/ml). Each bar depicts the mean ± standard deviation of 3 replicates from a representative donor (out of 4 donors tested in F and 3 donors in G), expressed as a percentage of the control treatment in the absence of antibiotic. Bars with solid colors represent Tamoxifen or control treatment only, bars with pattern represent the combination with antibiotic. Statistical significance was tested using a two-way ANOVA with Tukey's multiple comparisons test comparing Tamoxifen treatment (in the absence or presence of antibiotic) to the corresponding control treatment. (* = p<0.05, ** = p<0.01, *** = p<0.001 and **** = p<0.0001).

did not affect *Stm* growth, while the control anti-*Stm* antibiotic gentamicin completely prevented bacterial proliferation (Figure 1D).

Host-directed drugs are expected to work irrespective of the exact mycobacterial sub-strain targeted, including drug-susceptible and multi-drug resistant (MDR) *Mtb* strains. Since Tamoxifen demonstrated similar efficacy in both Mφ1 and Mφ2 we decided to

focus further on Mφ2 cells. Tamoxifen treatment of Mφ2 infected with two MDR-*Mtb* strains, *Mtb* Dutch outbreak strain 2003-1128 and *Mtb* Beijing strain 16319, significantly inhibited bacterial outgrowth in both cases (Figure 1E).

Additionally, since HDT molecules and classical antibiotics by definition target different molecules, positive interactivity might be anticipated during combined treatment. Indeed, Tamoxifen combined with a suboptimal dose of rifampicin (0.05 µg/ml) inhibited bacterial outgrowth more effectively than either molecule individually (Figure 1F). However, this effect was not observed when Tamoxifen was combined with a suboptimal dose of Isoniazid (0.4 µg/ml) (Figure 1G), suggesting that the effect of interactivity depends on the particular combination of Tamoxifen with antibiotics.

Taken together, we report strong HDT activity of Tamoxifen against both intracellular *Mtb* and *Stm*, in primary human macrophages regardless of their M1 or M2 polarization state. Furthermore, we demonstrate that Tamoxifen shows efficacy against both drug sensitive (DS)-*Mtb* and MDR-bacteria (*Mtb),* and that it might be used as adjunctive to classical antibiotics like Rifampicin.

In vivo validation of Tamoxifen as HDT

To investigate the efficacy of Tamoxifen *in vivo*, we employed the well characterized zebrafish TB model, in which embryos are infected with their natural pathogen *Mycobacterium marinum*. We first validated Tamoxifen's efficacy on *Mm* employing the

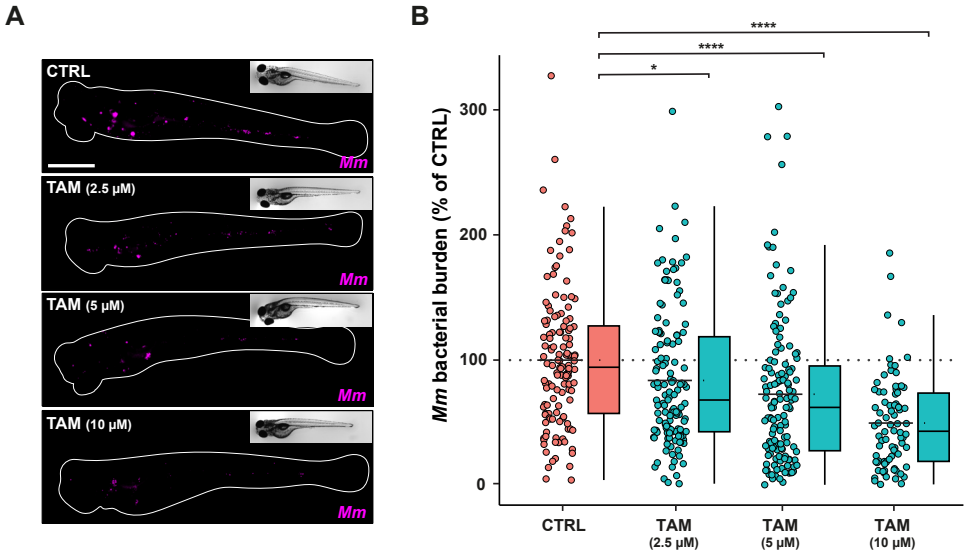

Figure 2. *In vivo* validation of Tamoxifen as HDT

A. Bacterial burden assay of mWasabi-expressing *Mm*-infected zebrafish larvae treated with increasing doses of Tamoxifen (2.5, 5 and 10 µM) or control (DMSO at 0.1% v/v). Treatment was started at 1 hpi and larvae anesthetized at 4dpi for imaging. Representative stereo fluorescent images of whole larvae infected with mWasabi-expressing *Mm*. Magenta shows *Mm*. Scale bar annotates 1 mm.

B. Quantification of bacterial burden shown in A. Bacterial burden was normalized to mean of the control, set at 100% and indicated with the dotted line. Data of 4 experimental repeats were combined (n = 132-139 per group). Each dot represents a single larva. Boxplots with 95% confidence intervals are shown and the black line in the boxplots indicates the group median, while the black line in the dot plot indicates the group mean. Statistical analysis was performed using a Kruskal-Wallis with Dunn's multiple comparisons test.

Figure and figure legend continued on next page.

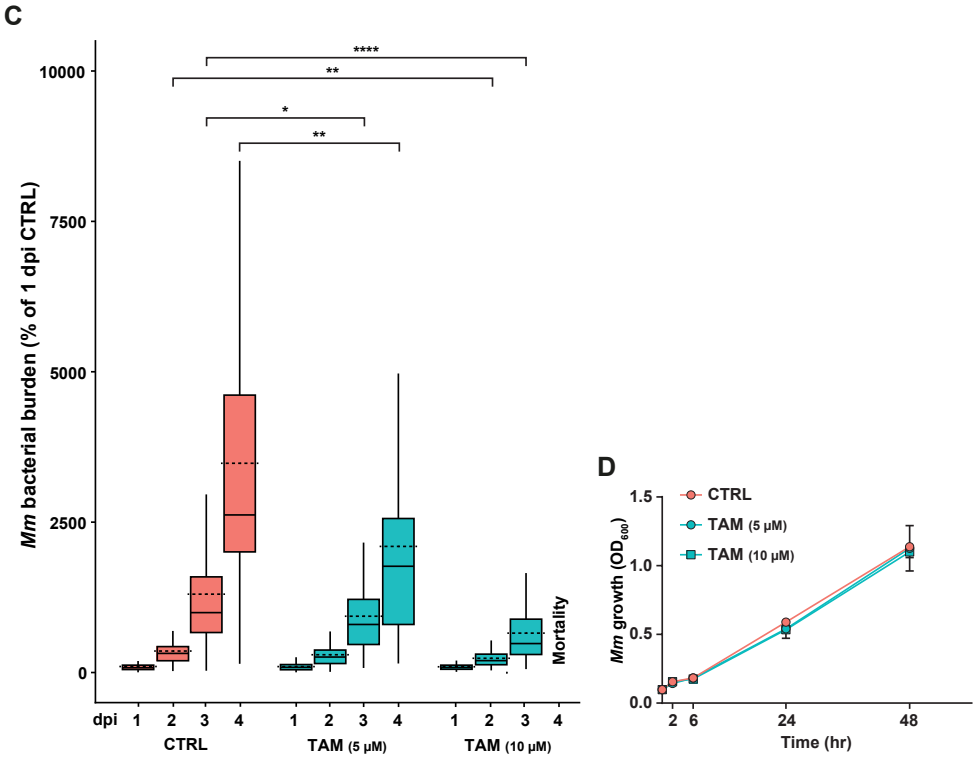

Figure 2. (continued)

C. Bacterial burden assay of mWasabi-expressing *Mm*-infected zebrafish larvae treated with 5 and 10 µM of Tamoxifen or control (DMSO at 0.1% v/v). Treatment was started at 1 hpi and larvae were anesthetized at 1, 2, 3 and 4 dpi for imaging. Bacterial burden was normalized to the control (DMSO at 1dpi) and data of 2 experimental repeats were combined (n = 65-70 per group). All larvae in the 10 µM group died between 3-4 dpi. Boxplots with 95% confidence intervals are shown and the black line in the boxplots indicates the group median, while the dotted line indicates the group mean. Statistical analysis was performed between treatment groups per timepoint using a Kruskal-Wallis with Dunn's multiple comparisons test.

D. *Mm* growth in liquid culture during treatment with 5 or 10 µM of Tamoxifen or control (DMSO at equal v/v) up to assay endpoint, day 2. Lines depict mean ± standard deviation of 2 experiments. Statistical significance of treatment versus control treatment was tested using a two-way ANOVA with Dunnett's multiple comparisons test.
(* = p<0.05, ** = p<0.01, *** = p<0.001 and **** = p<0.0001).

same flow-cytometry-based assay as used in the initial screen of HDT candidates for *Mtb*. As anticipated, Tamoxifen reduced *Mm* burden in human cells (Supplementary Figure 1). Next, we infected zebrafish embryos with mWasabi-labelled *Mm* and treated the infected embryos for 4 days with an increasing dose (2.5, 5 and 10 µM) of Tamoxifen or with vehicle (DMSO) control. Treatment with the highest dose (10 µM) resulted in developmental toxicity (e.g. oedema and lethality) in one third of the larvae, while no toxicity was observed at the lower doses. Bacterial burden was assessed by quantifying the bacterial fluorescence signal of infected larvae at 4 days post infection (dpi). All doses of Tamoxifen treatment reduced bacterial burden significantly compared to the control treatment in a dose-dependent manner (Figure 2A,B).

Next, we investigated the infection dynamics during treatment. We infected and treated embryos with Tamoxifen (5 and 10 µM) and imaged them daily for 4 days to monitor the establishing infection. Tamoxifen treatment reduced bacterial burden compared to

the control treatment from 2 dpi onward (Figure 2C). While drug-induced mortality was observed in the 10 µM group at experimental end point (4 dpi), Tamoxifen treatment with 5 µM resulted in an approximately 2-fold lower infection burden compared to the control treatment (DMSO) at 4 dpi (Figure 2C). Nonetheless, we observed that the infection burden increased between 2 and 4 dpi irrespective of treatment, indicating that Tamoxifen limits but does not fully inhibit bacterial growth.

Although we had found Tamoxifen to work as HDT on *Mtb*-infected cells *in vitro*, we sought to exclude that its effect in the zebrafish TB model was due to a direct antibacterial reduction of *Mm* growth as opposed to a host-directed effect. Therefore, we added Tamoxifen at doses of 5 and 10 µM to a liquid culture of *Mm* and assessed bacterial replication by measuring optical density (OD_{600}) at 5 time points starting from 2 hours until experimental endpoint (48 hours). No change in *Mm* growth rate could be observed (Figure 2D), confirming that the observed reduction of bacterial burden in zebrafish larvae is due to a host-directed and not a direct anti-bacterial effect of Tamoxifen. For further experiments in our *in vivo* TB model, we used Tamoxifen at 5 µM as this dose consistently lowered bacterial burden in zebrafish larvae in a host-directed manner, without causing developmental toxicity.

Tamoxifen alters leukocyte-specific gene expression without affecting macrophage or neutrophil migration *in vivo*

We decided to use the zebrafish TB model to investigate the host transcriptomic response to Tamoxifen treatment at a systemic level to obtain mechanistic insight into the observed inhibition of mycobacterial infection. Using RNA sequencing analysis, we compared the effects of Tamoxifen or DMSO control treatments on the transcriptomes of infected larvae at 2 dpi (3 dpf) and non-infected control larvae. Following quality control analysis and data processing (Supplementary Figure 2A-G), we analyzed the differential expression of transcripts in infected compared to non-infected larvae, in the absence of Tamoxifen. We found 204 genes to be differentially expressed during mycobacterial infection at 2 dpi (Supplementary Data File 1), including upregulation of the matrix metalloproteinase genes *mmp13a* and *mmp9* (Supplementary Figure 3A), which is consistent with earlier transcriptomic data of *Mm*-infected zebrafish at the same time point after infection[46]. Tamoxifen treatment of non-infected larvae caused differential expression of 141 genes, including genes involved in ER signaling and autophagy and other cellular stress pathways, consistent with known effects of Tamoxifen exposure[23,24,30,47-49] (Supplementary Data File 1)

Next, we analyzed the genes that showed interaction between Tamoxifen treatment and infection – that is genes whose expression during infection was altered by Tamoxifen treatment – and found 28 significant up- or down-regulated genes (Supplementary Table S2). These differential transcriptomic responses could be due to the lower bacterial burden in Tamoxifen-treated larvae during infection compared to the control group. For example, the lower upregulation of *mmp9* and *mmp13a* during Tamoxifen treatment is in line with a reduced inflammatory response in larvae with lower infection burden (Supplementary Figure 3A). However, we also found alterations in leukocyte-specific marker genes that were dependent on Tamoxifen treatment, such as *marco* and *mfap4*, suggesting that the number of leukocytes or their behavior during infection could be altered due to Tamoxifen treatment (Supplementary Figure 3B). Furthermore, we found 14 genes that were differentially regulated by both Tamoxifen treatment and infection compared to their respective control larvae (Supplementary Figure 3C and Supplementary Table S3). Interestingly, several of these 14 genes were related to immune processes (*cp*, *ccl34a*) (Supplementary Figure 3D) or highly expressed in leukocytes

(*mpx*, *grna*, *mfap4*) (Supplementary Figure 3E). This indicated that Tamoxifen treatment could modulate the cellular immune response even in the absence of infection. Together, these data correlate the decrease in bacterial burden in Tamoxifen-treated larvae with modulation of inflammatory responses and leukocyte development or behavior.

The development of *Mm* infection in zebrafish larvae depends strongly on migratory responses of macrophages and neutrophils, which aggregate to form the initial stages of TB granulomas[50-52]. In addition to transcriptional effects on leukocyte markers detected in our study, Tamoxifen has been reported to both inhibit and stimulate neutrophil migration[53-55]. Therefore, we asked if leukocyte migration was altered upon Tamoxifen treatment in our model. To this end we used an established injury-based migration assay, the tail amputation assay[56] in a double transgenic neutrophil and macrophage marker line and assessed the number of neutrophils and macrophages that migrated to the wound-induced site of inflammation. We did not find a significant difference between control or Tamoxifen treated groups in both neutrophil and macrophage numbers that migrated towards the injury (Supplementary Figure 3F-H). In conclusion, despite transcriptional changes in leukocyte-specific genes caused by Tamoxifen treatment, we did not detect altered leukocyte behavior in response to an inflammatory stimulus. Therefore, we decided to focus next on analysing the broad systemic effects of Tamoxifen treatment detected in the RNA sequencing analysis, specifically in relation to estrogen receptor (ER)-signaling and autophagy, processes both known to be modulated by Tamoxifen.

The host-directed effect of Tamoxifen is independent of ER signaling

The ER is the most well-characterized target of Tamoxifen. Tamoxifen is known to have a dual role, and can act both as an agonist and as an antagonist of ER signaling[23]. We therefore investigated whether modulating ER signaling by selective ER-agonistic and antagonistic compounds would affect bacterial burden, and in which direction. Human Mφ2 cells were infected with *Mtb* and treated with the ER agonists 17α-estradiol or 17β-estradiol, and bacterial outgrowth was measured by CFU. While Tamoxifen reduced *Mtb* growth by approximately 50% compared to control DMSO, neither ER agonist consistently affected *Mtb* growth, regardless of the concentration used (Figure 3A). Since Tamoxifen effects may depend on sex differences[57], and macrophage ER receptor levels differ between sexes[58], we investigated whether human donor sex influenced Tamoxifen HDT activity in primary macrophages from male vs. female donors. No significant differences in Tamoxifen's efficacy against intracellular bacteria were observed between male and female primary macrophages (Figure 3B).

Next, we studied if ER signaling is responsible for the effect of Tamoxifen on *Mm* infection *in vivo*. First, we used our zebrafish transcriptome data to identify classes of differentially expressed genes associated with Tamoxifen treatment by performing Gene Set Enrichment Analysis (GSEA)[59]. Tamoxifen-treated larvae showed downregulation of genes normally upregulated by 17β-estradiol, while genes that are normally downregulated by this ER agonist were upregulated after Tamoxifen treatment (Figure 3C). Considering this large effect of Tamoxifen on ER target genes, we investigated whether activating or blocking ER signaling *in vivo* would result in a similar reduction of bacterial burden as Tamoxifen treatment. We first used 17β-estradiol to activate ER signaling during *Mm* infection. To verify the effect of this agonist, we analyzed the expression level of two ER target genes, *vtg1* and *cyp19a1b*, by qPCR. After 17β-estradiol treatment (0.1, 1 and 5 μM), both infected and non-infected larvae showed markedly increased expression levels of *cyp19a1b* (reaching approx. 10-fold at the highest 17β-estradiol dose) and *vtg1* (approx. 100-fold at the 1 μM dose), while upregulation of these genes was not detected following treatment with Tamoxifen compared to

the control treatment (Figure 3D). Despite activation of ER signaling, no reduction in bacterial burden could be observed following 17β-estradiol treatment, while treatment with Tamoxifen reduced bacterial burden significantly compared to the control (Figure 3E). These results led us to consider the possibility that the effect on bacterial burden after Tamoxifen treatment might be due to the ER antagonistic role of Tamoxifen. Therefore, we investigated whether we could reproduce the effect of Tamoxifen using

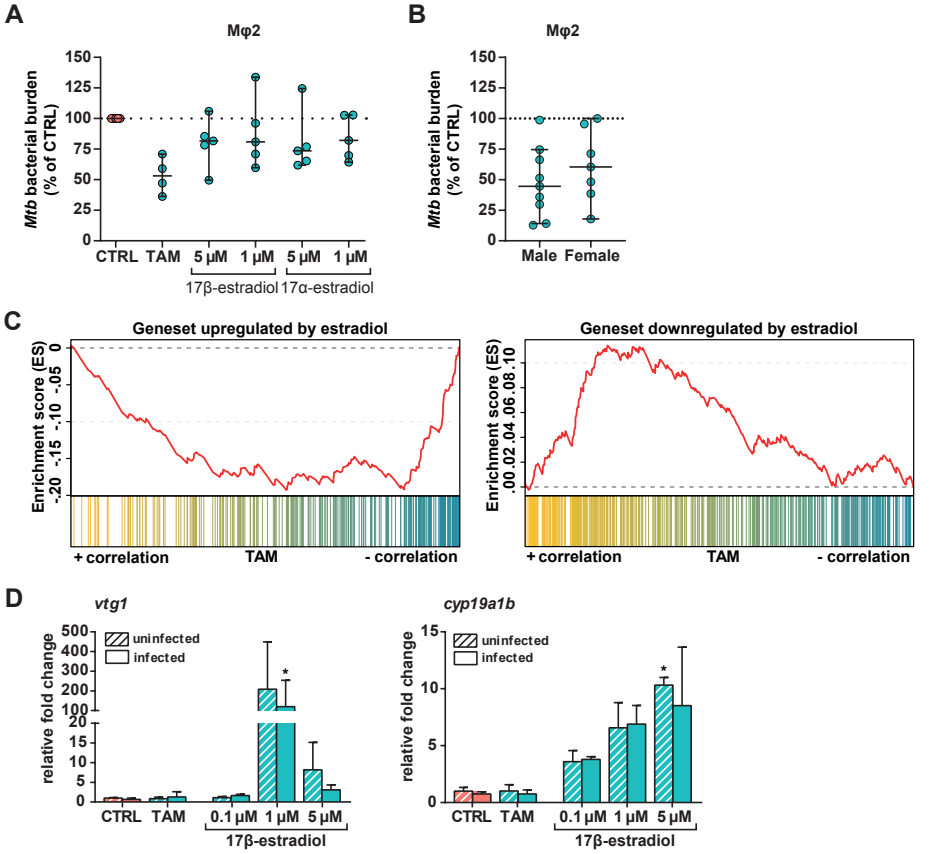

Figure 3. The host-directed effect of Tamoxifen is independent of ER-signaling

A. CFU assay of Mφ2 infected with H37Rv-*Mtb* and treated with Tamoxifen (10 µM), 17β-Estradiol (1 or 5 µM), 17α-Estradiol (1 or 5 µM) or control (DMSO at equal v/v) for 24 hours. Each dot represents a single donor (4 to 5 donors were tested) and depicts the mean of 3 replicates normalized to control. Dotted line indicates control set at 100% and median + 95% confidence intervals are shown for every condition. Statistical significance was tested using Wilcoxon matched-pairs signed rank test with post-hoc Benjamini-Hochberg correction.

B. CFU assay of Mφ2 infected with H37Rv-*Mtb* and treated with 10 µM of Tamoxifen for 24 hours, separated for donor sex. The graph includes data points from Figure 1A and Figure 3A. Each dot represents a single donor (9 in male group, 7 in female group) and depicts the mean of 3 replicates normalized to control. Dotted line indicates control set at 100% and median + 95% confidence intervals are shown for every condition. Statistical significance was tested using a Mann-Whitney U test.

C. GSEA enrichment plots of downregulated (left panel) and upregulated (right panel) estradiol-responding genes in zebrafish larvae treated with 5 µM of Tamoxifen for 2 days (3 dpf). All estradiol-responding genes in the Tamoxifen-treated larval transcriptome were ranked according to their statistical significance and direction of regulation, from left (most significant, upregulated in yellow) to right (most significant, downregulated in blue). Each column depicts the position of an individual gene belonging to the gene set of estradiol-responding genes in the ranked list.

Figure and figure legend continued on next page.

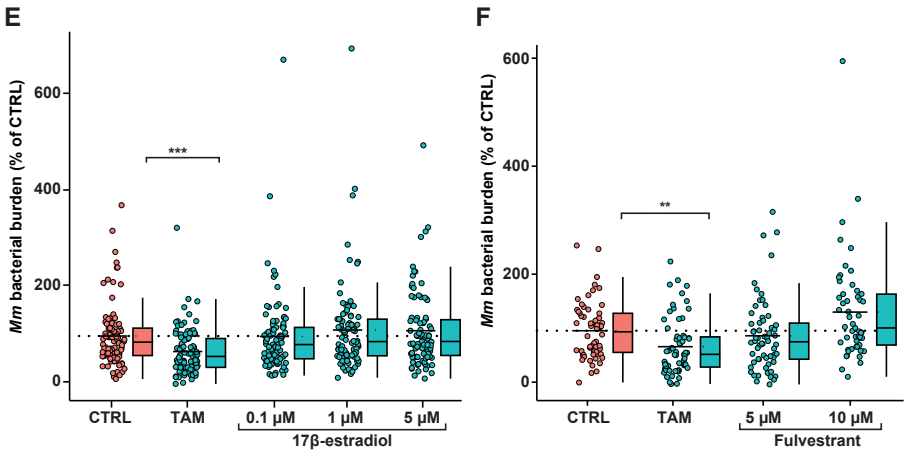

Figure 3. (continued)

D. Non-infected and mWasabi-expressing *Mm*-infected zebrafish larvae were treated with 5 µM of Tamoxifen, increasing doses of ER agonist 17β-estradiol (0.1, 1 and 5 µM) or control (DMSO at 0.05% v/v) starting 1 hpi. Transcript levels of two β-estradiol-responsive genes, *vtg1* (left graph) and *cyp19a1b* (right graph) were determined by qPCR analysis at 4 dpi. Data were normalized to the expression of the housekeeping gene TATA box binding protein (*tbp*) and data of 3 biological replicates were combined (n = 10 larvae per replicate). Each bar depicts the average fold change (FC) of transcript levels relative to non-infected or infected control treated zebrafish larvae and the error bar indicates SEM. Statistical analysis was performed using a Kruskal-Wallis with Dunn's multiple comparisons test. Effect of treatment compared to control was analyzed within the non-infected and infected group separately.

E. Bacterial burden assay of mWasabi-expressing *Mm*-infected zebrafish larvae treated as in D. Treatment was started at 1 hpi and larvae anesthetized at 4 dpi for imaging. Bacterial burden was normalized to the control and data of 3 experimental repeats were combined (n = 93-95 per group). Each dot represents a single larva. Boxplots with 95% confidence intervals are shown and the black line in the boxplots indicates the group median, while the black line in the dot plot indicates the group mean. Dotted line indicates control mean set at 100%. Statistical analysis was performed using a Kruskal-Wallis with Dunn's multiple comparisons test.

F. Bacterial burden assay of mWasabi-expressing *Mm*-infected zebrafish larvae treated with of 5 µM of Tamoxifen, increasing doses of ER antagonist Fulvestrant (5 and 10 µM) or control (DMSO at 0.05% v/v). Treatment was started at 1 hpi and larvae were anesthetized at 4 dpi for imaging. Bacterial burden was normalized to control and data of 2 experimental repeats were combined (n = 53-63 per group). Each dot represents a single larva. Boxplots with 95% confidence intervals are shown and the black line in the boxplots indicates the group median, while the black line in the dot plot indicates the group mean. Dotted line indicates control mean set at 100%. Statistical analysis was performed using a Kruskal-Wallis with Dunn's multiple comparisons test.
(* = $p<0.05$, ** = $p<0.01$ and *** = $p<0.001$).

the ER antagonist Fulvestrant. However, we did not detect an effect on bacterial burden using two different doses of Fulvestrant (Figure 3F). In contrast, we even observed a trend towards an increase of bacterial burden with the higher dose of Fulvestrant (10 µM). These data indicate that even though Tamoxifen treatment alters the host transcriptome related to ER signaling, activating or blocking ER signaling does not enhance the host-response to mycobacterial infection, suggesting Tamoxifen controls bacterial burden via alternative mechanisms than ER signaling.

To provide further evidence that Tamoxifen indeed functions independently of ER signaling, we followed a genetic approach. Two ER subtypes, ERα and ERβ, are conserved in vertebrate evolution. In zebrafish, *esr1* encodes for the ERα subtype, while due to a gene duplication event, two ER-genes; *esr2a* and *esr2b,* encode for ERβ[60,61]. For our study, we took advantage of an available *esr2b* loss-of-function mutant, which previously has been shown to be impaired in its response to viral infection[62]. We observed reduced *Mm* bacterial burdens in all Tamoxifen treated groups compared

to the DMSO control treated groups independently of the *esr2b*$^{+/+}$, *esr2b*$^{+/-}$ or *esr2b*$^{-/-}$ genotype (Supplementary Figure 4). Together, the pharmacological and genetic data show that neither activating nor blocking ER signaling in zebrafish leads to reduction of bacterial burden, and that Esr2b is not required for the effect of Tamoxifen on bacterial burden.

Collectively, these data suggest that Tamoxifen's HDT-effect against intracellular bacteria is independent from ER signaling. In line with this result, ER agonists do not consistently affect intracellular *Mtb* growth, the activity of the ER pathway in zebrafish is not required for Tamoxifen's HDT-effect and its efficacy in primary macrophages is not affected by the sex of the donor.

Tamoxifen treatment modulates autophagy in infected human macrophages and zebrafish

Because Tamoxifen induces and modulates autophagy, and because autophagy contributes to host defense against TB, we next investigated the role of Tamoxifen-induced autophagy in inhibiting bacterial outgrowth[30,49,63]. We first employed CYTO-ID, a tracer for autophagy related vesicles offering the advantage of staining all intracellular autophagy-related vesicles independent of proteins such as LC3. Mφ2 were infected with *Mtb,* subsequently treated for 4 hours with Tamoxifen, stained with the CYTO-ID tracer and visualized using confocal microscopy (Figure 4A). Although differences did not reach the statistical significance threshold due to well-known variation between human donors, a clearly increasing trend in both area of Cyto-ID vesicles and the colocalization of *Mtb* with these vesicles was observed in response to Tamoxifen (Figure 4B).

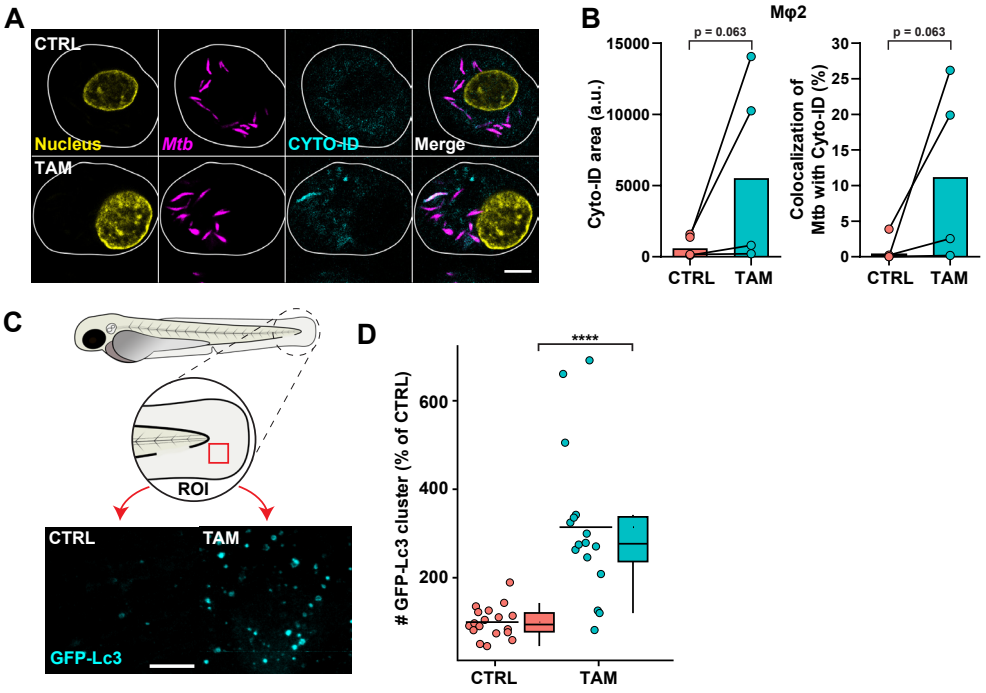

Figure 4. Tamoxifen treatment modulates autophagy in infected human macrophages and zebrafish

Figure and figure legend continued on next page.

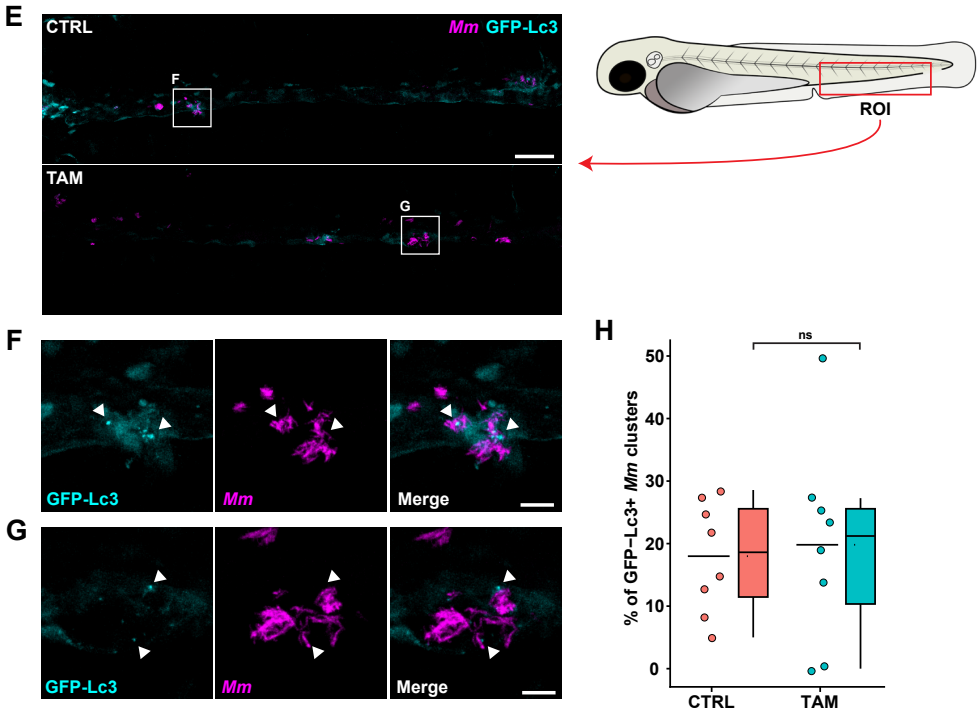

Figure 4. (continued)

A. Confocal microscopy of DsRed-expressing H37Rv-*Mtb*-infected Mφ2 treated with 10 µM of Tamoxifen or control (DMSO at equal v/v) for 4 hours. 30 min prior to the experimental endpoint cells were incubated with CYTO-ID to stain for autophagy related vesicles, fixed with 1% paraformaldehyde and counterstained for the nucleus using Hoechst 33342. In the representative images, yellow shows the nucleus, magenta shows *Mtb*, cyan shows autophagy related vesicles and the scale bar annotates 5 µm.

B. Quantification of Cyto-ID signals in A. The left panel displays Cyto-ID positive area, while the right panel displays *Mtb* colocalization with Cyto-ID positive vesicles. Each dot displays the mean of 3 or 4 replicates and represents a single donor (4 donors in total) with median indicated by colored bars. Statistical significance was tested using Wilcoxon matched-pairs signed rank test.

C. Confocal microscopy of transgenic GFP-Lc3 zebrafish larvae treated with 5 µM of Tamoxifen or control (DMSO at equal v/v). Treatment was started at 3 dpf and larvae were fixed with 4% paraformaldehyde at 4 dpf for imaging. Representative max projection images of GFP-Lc3 positive vesicles in the indicated region of imaging (ROI) in the tail fin are shown. Cyan shows GFP-Lc3 positive vesicles. Scale bar annotates 10 µm.

D. Quantification of GFP-Lc3 structures shown in C. Data were normalized to the control and data of 2 experimental repeats were combined (n = 16-18 per group). Each dot represents a single larva. Boxplots with 95% confidence intervals are shown and the black line in the boxplots indicates the group median, while the black line in the dot plot indicates the group mean. Statistical analysis was performed using a Mann Whitney test.

E. Confocal microscopy of mCherry-expressing *Mm*-infected transgenic GFP-Lc3 zebrafish larvae treated with 5 µM of Tamoxifen or control (DMSO at equal v/v). Treatment was started at 1 hpi and at 2 dpi larvae were fixed with 4% paraformaldehyde for imaging. Representative max projection images of the ROI in the caudal hematopoietic tissue (CHT) region are shown. Cyan shows GFP-Lc3 positive vesicles and magenta shows *Mm*. Scale bar annotates 50 µm.

F-G. Enlargement of areas indicated in E. Cyan shows GFP-Lc3 positive vesicles and magenta shows *Mm*. Arrowheads indicate GFP-Lc3-positive *Mm* clusters. Scale bar annotates 10 µm.

H. Quantification of GFP-Lc3 positive *Mm* clusters in the CHT region shown in E normalized to the control (n = 8 per group). Each dot represents a single larva. Boxplots with 95% confidence intervals are shown and the black line in the boxplots indicates the group median, while the black line in the dot plot indicates the group mean. Statistical analysis was performed using a Mann Whitney test.
(**** = p<0.0001).

We further explored the role of autophagy using a fluorescent zebrafish reporter line for Lc3[64]. Zebrafish larvae (3dpf) were treated with Tamoxifen for 24 hours and theGFP-Lc3 response was visualized in the thin tissue of the larval tail fin, which is well suited for using confocal microscopy (Figure 4C)[41]. We observed a significant increase in GFP-Lc3 positive structures in the Tamoxifen treated group compared to control treatment (Figure 4D), consistent with an autophagy modulating effect of Tamoxifen. In contrast, neither the ER agonist 17β-estradiol nor the ER antagonist Fulvestrant showed an increase in GFP-Lc3 positive structures (Supplementary Figure 5A,B). Therefore, we conclude that Tamoxifen modulates autophagy in the zebrafish model by an ER-independent mechanism. Next, to study whether Tamoxifen increased co-localization between GFP-Lc3 structures and *Mm*, we infected 1 dpf embryos of the GFP-Lc3 reporter line and imaged them at 2 dpi in their caudal hematopoietic tissue (CHT), a preferred location for aggregation of infected macrophages, the initial step in tuberculous granuloma formation[50]. We observed *Mm* clusters distributed from the injection site to the end of the tail and various GFP-Lc3 positive structures colocalized with these clusters (Figure 4E-G). However, we found no significant differences in the percentage of *Mm* clusters positive for GFP-Lc3 structures between control and Tamoxifen treatment (Figure 4H).

In summary, Tamoxifen treatment increased the abundance of autophagy vesicles both *in vitro* and *in vivo*, but the effects on colocalization of these vesicles with mycobacteria were modest or undetectable. This suggests that the autophagy induction by Tamoxifen might play a secondary or temporary role in decreasing mycobacterial infection.

Tamoxifen treatment alters lysosomal function and increases mycobacterial lysosomal localization *in vitro* and *in vivo*

Since mycobacteria can be targeted to lysosomes both dependent and independent of autophagy, we investigated whether vesicle maturation was affected by Tamoxifen. Therefore, a tracer for lysosomes, LysoTracker, was used to quantify acidic vesicles. Mφ2 were infected with *Mtb,* subsequently treated for 4 hours with Tamoxifen, stained with LysoTracker, and visualized using confocal microscopy (Figure 5A). Tamoxifen consistently and significantly increased both LysoTracker area and the colocalization of

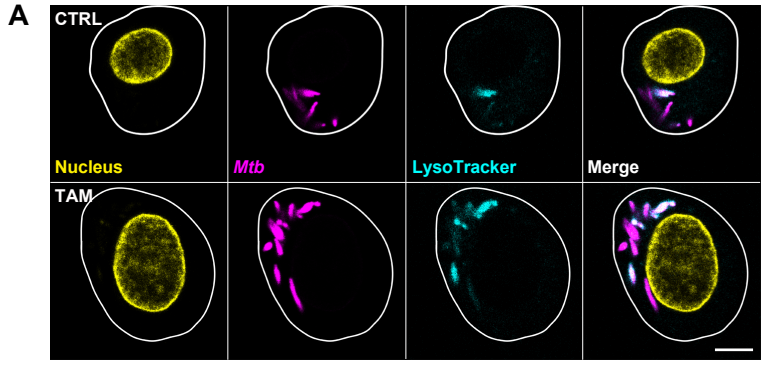

Figure 5. Tamoxifen treatment alters lysosomal function and increases mycobacterial lysosomal localization *in vitro* and *in vivo*

A. Confocal microscopy of DsRed-expressing H37Rv-*Mtb*-infected Mφ2 treated with 10 μM of Tamoxifen or DMSO at equal v/v for 4 hours. 30 min prior to the experimental endpoint cells were incubated with LysoTracker Deep Red to stain for acidic vesicles, fixed with 1% paraformaldehyde and counterstained for the nucleus using Hoechst 33342. In the representative images, yellow shows the nucleus, magenta shows *Mtb*, cyan shows acidic vesicles and the scale bar annotates 5 μm.

Figure and figure legend continued on next page.

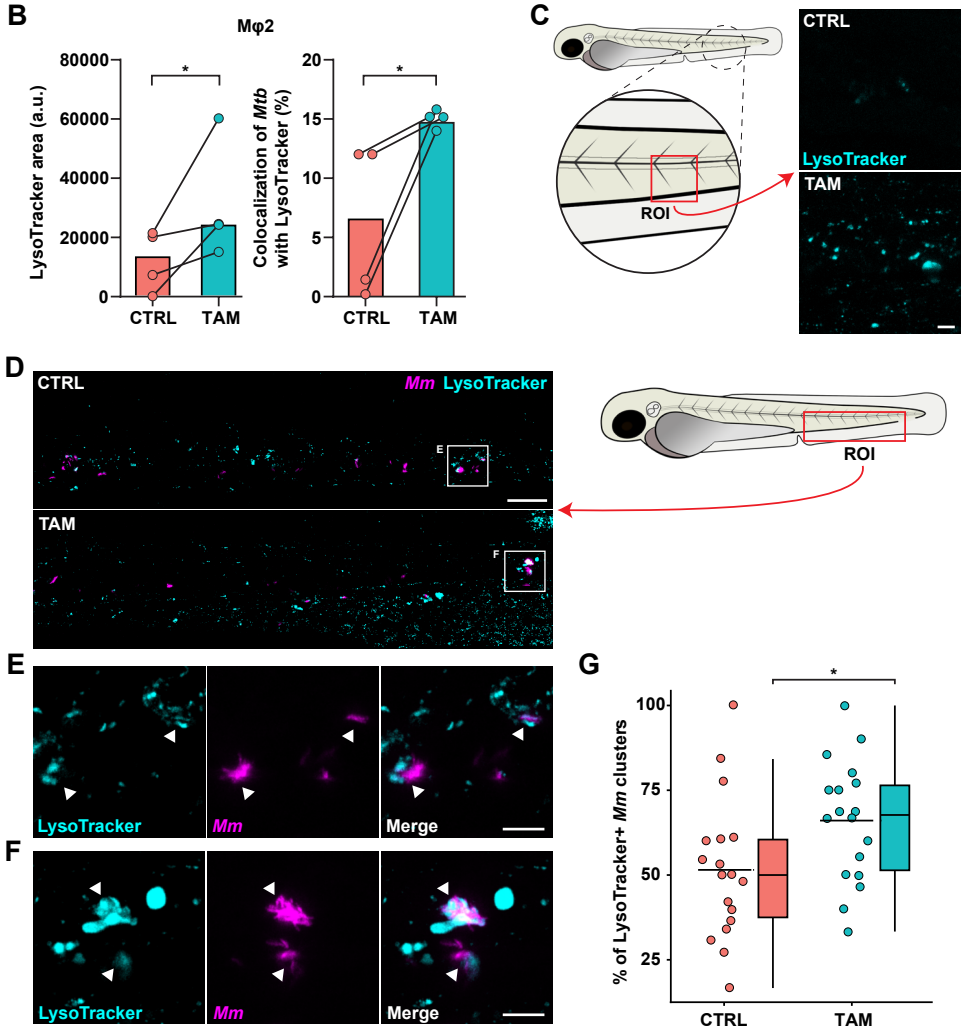

Figure 5. (continued)

B. Quantification of LysoTracker signal in A. The left panel displays Lysotracker positive area, while the right panel displays *Mtb* colocalization with Lysotracker positive vesicles. Each dots displays the mean of 3 or 4 replicates and represents a single donor (4 donors in total) with median indicated by colored bars. Statistical significance was tested using a paired T test.

C. Confocal microscopy max projection of the indicated ROI in zebrafish larvae treated with 5 µM of Tamoxifen or control (DMSO at equal v/v). Treatment was started at 31 hpf and at 3 dpf larvae were immersed in 5 µM of LysoTracker Red DND-99 for 1 hour and subsequently anesthetized for imaging. Cyan shows acidic vesicles. Scale bar annotates 10 µm.

D. Confocal microscopy max projection of mWasabi-expressing *Mm*-infected zebrafish larvae treated with 5 µM of Tamoxifen or control (DMSO at equal v/v). Treatment was started at 1 hpi and at 2 dpi larvae were immersed in 5 µM of LysoTracker Red DND-99 for 1 hour and subsequently anesthetized for imaging. Representative max projection images of LysoTracker positive *Mm* clusters in the CHT region are shown. Cyan shows acidic vesicles and magenta shows *Mm*. Scale bar annotates 50 µm.

E-F. Enlargement of areas indicated in D. Cyan shows acidic vesicles and magenta shows *Mm*. Arrowheads indicate LysoTracker positive *Mm* clusters. Scale bar annotates 10 µm.

G. Quantification of LysoTracker-positive *Mm* clusters normalized to the control and data of 3 experimental repeats were combined (n = 18 per group). Each dot represents a single larva. Boxplots with 95% confidence intervals are shown and the black line in the boxplots indicates the group median, while the black line in the dot plot indicates the group mean. Statistical analysis was performed using a Mann Whitney test. (* = $p<0.05$).

Mtb with LysoTracker (Figure 5B), suggesting that Tamoxifen's effect on the lysosomal response is relevant for *Mtb* infection.

In line with these results, further analysis of our zebrafish transcriptome data by means of pathway enrichment against the KEGG database revealed phagosome and lysosome pathways as strongly enriched in response to Tamoxifen treatment (Supplementary Table S4). In addition, Gene Ontology and Gene Set Enrichment Analysis (GSEA) highlighted that genes with molecular functions such as hydrolase and peptidase activity, biological processes such as proteolysis, and genes belonging to the lysosome compartment were enriched in response to Tamoxifen treatment (Supplementary Table S4). In fact, lysosomal genes such as vATPases, cathepsins and *lamp1* were all upregulated in the transcriptome of Tamoxifen treated larvae (Supplementary Data File 1). We therefore asked whether Tamoxifen treatment could also increase the localization of *Mm* clusters in lysosomes *in vivo*. Thus, we treated embryos with Tamoxifen or DMSO starting at 1 dpf (1 hpi) for 2 days and performed LysoTracker staining at 2 dpi (3 dpf). A strong increase in LysoTracker signal intensity was observed independent of infection (Figure 5C). Furthermore, imaging of the CHT region of infected larvae (Figure 5D-F) showed an increase in the colocalization between LysoTracker signal and *Mm* clusters from 50% in the control group to 65% in Tamoxifen-treated larvae (Figure 5G), corroborating the transcriptome results that Tamoxifen modulates lysosomal activity.Taken together, both in primary human macrophages and in zebrafish we observed increased LysoTracker signal intensity following treatment with Tamoxifen. Importantly, Tamoxifen led to enhanced targeting of *Mtb* and *Mm* to LysoTracker positive vesicles in these *in vitro* and *in vivo* infection models. Finally, this effect of Tamoxifen treatment was associated with modulated lysosomal gene expression. These data lead us to propose that Tamoxifen treatment reduces infection burden during mycobacterial infection by a host-dependent increase of lysosomal activity.

Discussion

The concept of HDT, combatting infection with drugs that empower the immune system, is increasingly explored as alternative or adjunctive therapeutic approaches against *Mtb* strains that are unresponsive to classical antibiotics[13-15,21], we demonstrate that the breast-cancer therapy drug Tamoxifen, restricts bacterial outgrowth of *Mtb* in primary human macrophages of different inflammatory states and differentiation stages. Furthermore, Tamoxifen shows high efficacy against clinical isolates of MDR-TB and is also active against *Stm*. Importantly, using *Mm*-infected zebrafish larvae as an *in vivo* TB model, we further substantiated the repurposing potential of Tamoxifen as an HDT for TB. Furthermore, we showed that Tamoxifen reduces bacterial burden independent of ER signaling and propose that the HDT effect of Tamoxifen is mediated primarily by enhancing lysosomal degradation pathways.

Tamoxifen has been proposed as a new antibiotic, because it was found to have direct antibacterial effects against intracellular pathogens[26-28]. Tamoxifen antimicrobial activity against *Mtb* was found at doses ranging from 16.7 to 26.8 μM, whereas lower doses similar to the ones used in our study lacked significant effects[28,29]. In agreement with this, when using Tamoxifen in low doses up to 10 μM, we did not observe any direct effect on either *Mtb*, *Stm* or *Mm* growth in liquid cultures. Importantly, both *Mtb* and *Stm* outgrowth and *Mm* burden in infected human macrophages and zebrafish larvae, respectively, were inhibited effectively by Tamoxifen at these doses (5-

10 μM). Therefore, we propose Tamoxifen as a potential new HDT against (myco-) bacterial infection. Recently, a structurally and functionally related breast-cancer drug, Bazedoxifene, has also been proposed as an HDT for TB, supporting the therapeutic potential of this class of chemicals[65]. The therapeutic potential of these drugs may extend to a wide range of bacterial pathogens, as Tamoxifen was recently found to have an immunomodulatory effect against MDR gram-negative bacilli, including *Acetinobacter baumannii*, *Pseudomonas aeruginosa*, and *Escherichia coli*[66].

The best-known target of drugs like Tamoxifen and Bazedoxifene is the ER[23,24]. However, our data do not support a role for the ER in mediating the anti-mycobacterial function of Tamoxifen. ER agonists did not significantly affect bacterial outgrowth *in vitro* and donor sex did not affect Tamoxifen restricted *Mtb* outgrowth in our model, despite that sex-based differences both in macrophage ER receptor amounts and differential effects of Tamoxifen treatment have been reported[57,58]. Furthermore, although zebrafish transcriptome analysis showed that Tamoxifen antagonized ER-signaling, Tamoxifen reduced *Mm* burden in *esr2b* mutants, indicating that its HDT effect is independent of the Esr2b receptor. Although we cannot exclude the involvement of other zebrafish ER receptors (*esr2a* and *esr1*), we considered the Esr2b receptor a prime candidate for mediating a potential HDT effect of Tamoxifen because an *esr2b* loss-of-function mutant has previously been linked to a host defense phenotype[62]. Finally, chemical activation and inhibition of ER-signaling using 17β-estradiol and Fulvestrant, respectively, did not affect mycobacterial burden while they are known to affect ER signaling in zebrafish[67,68]. Of note, we show several other host pathways, including autophagy and lysosome function to be modulated by Tamoxifen, in addition to ER-signaling. Thus, we propose that ER-independent host-directed effects of Tamoxifen are responsible for the reduction of bacterial burden.

The autophagy-inducing function of Tamoxifen, demonstrated in several previous studies[30,49], could be a plausible explanation for its anti-mycobacterial effect, considering that activating autophagy reduces mycobacterial burden both *in vitro* and *in vivo*[19,40], while impaired autophagy during mycobacterial infection is detrimental to the host[42,69,70]. Of note, the anti-TB effect of the related drug Bazedoxifene was attributed to its autophagy inducing properties, dependent on AKT/mTOR signaling and the production of mitochondrial reactive oxygen (ROS) species[65]. The authors proposed that Bazedoxifene suppresses *Mtb* outgrowth in macrophages by enhancing autophagosome formation, as chemical or genetic inhibition of autophagy reduced the antibacterial effect. Likewise, we also observed an autophagy increasing effect of Tamoxifen, which might similarly be related to mitochondrial ROS production, as our transcriptome data indicated a mitochondrial stress response, which is a well-known effect of Tamoxifen[47,48]. However, while our results suggested increased *Mtb* localization in Cyto-ID positive vesicles *in vitro*, we were unable to demonstrate an increase in the colocalization of *Mm* with the autophagy marker GFP-Lc3 *in vivo*. This might be explained by both the transient nature of GFP-Lc3-*Mm* associations and the properties of the tracer Cyto-ID, since next to autophagosomes it also stains autophagolysosomes[71], thus possibly reflecting mature lysosomes with degraded LC3. Taken together, it remains possible that increased autophagosome formation contributes to the HDT effect of Tamoxifen but, based on our data on autophagy and on the lysosomal responses we favor the hypothesis that Tamoxifen restricts mycobacterial growth primarily by augmenting the (auto)phagosome maturation process that delivers bacteria to lysosomes.

The clearance of (auto)phagosomes, as well as the delivery of neo-antimicrobial peptides, depends on the fusion with lysosomes resulting in autophagolysosomes or

phagolysomes[16,72,73]. Even in the absence of infection, the transcriptome of Tamoxifen-treated zebrafish showed major modulation of lysosomal function. Although studies in breast cancer cells have shown that Tamoxifen inhibits lysosomal acidification early during treatment due to its lysosomotrophic behavior[74-76], importantly, this rapidly triggers lysosomal activation that within hours restores pH and increases lysosomal volume to a level higher than prior to treatment[76]. In agreement, LysoTracker signal increased after Tamoxifen treatment in both human macrophages and zebrafish larvae. This appears to have a positive effect on infection control, as we observed increased colocalization between LysoTracker signal and both *Mtb in vitro* and *Mm* clusters *in vivo*. Based on these results, we propose that the primary mechanism underlying Tamoxifen's ability to restrict mycobacterial infection is an increase of bacterial sequestration to the lysosome due to *de novo* lysosomal biogenesis.

Taken together, our results suggest that the increase in lysosomal activation by the lysosomotrophic drug Tamoxifen empowers the host to better control intracellular infection with various intracellular pathogens, including *Mtb* and *Stm*, and that this underlies the host-mediated therapeutic effect observed in mycobacterial *in vitro* and *in vivo* infection models. This therapeutic effect, which enhances the killing capacity of macrophages, may be augmented by other immunomodulatory functions of Tamoxifen, recently described, including the reduction of inflammatory cytokine release and the stimulation of neutrophil extracellular trap formation[66,77]. Treatment with Tamoxifen vastly reduced *Mtb* outgrowth in primary human macrophages, while in combination with a low dose of Rifampicin affected *Mtb* outgrowth with close to a 2-log reduction. Importantly, 4 days of Tamoxifen monotherapy in the zebrafish model for TB achieved an average reduction of the overall infection load by 30%. Tamoxifen is therefore a prime candidate for further evaluation as an adjunctive therapy to classical antibiotics, particularly for MDR- and XDR-TB.

Materials and methods

Chemicals

Tamoxifen citrate (Tamoxifen) and rifampicin were purchased from Sigma-Aldrich, Zwijndrecht, The Netherlands. Isoniazid was purchased from SelleckChem, Munich, Germany. Gentamicin sulfate was bought from Lonza BioWhittaker, Basel, Switzerland and Hygromycin B was acquired from Life Technologies-Invitrogen, Bleiswijk, The Netherlands. Fulvestrantand 17β-estradiol were bought from Sigma-Aldrich. All compounds, except Gentamicin sulfate and Hygromycin B, were dissolved in 100% dimethyl sulfoxide (DMSO, Sigma-Aldrich) in stock concentrations of 10mM, aliquoted and kept at -80 °C.

Primary macrophage culture

Buffy coats were obtained from healthy donors after written informed consent (Sanquin Blood Bank, Amsterdam, The Netherlands). Peripheral blood mononuclear cells (PBMCs) were purified using density gradient centrifugation over Ficoll-Paque and monocytes isolated with subsequent CD14 MACS sorting (Miltenyi Biotec, Bergisch Gladsbach, Germany) as described previously[34,35]. Monocytes were then differentiated into pro-inflammatory (Mφ1) or anti-inflammatory (Mφ2) macrophages with 5 ng/ml of granulocyte-macrophage colony-stimulating factor (GM-CSF; Life Technologies-Invitrogen) or 50 ng/ml macrophage colony-stimulating factor (M-CSF; R&D Systems, Abingdon, UK), respectively, for 6 days with a cytokine boost at 3 days, as previously

reported[44]. Cells were cultured at a density of 1×10^6 cells per ml in T75 flasks at 37°C/5% CO_2 in Gibco Roswell Park Memorial Institute (RPMI) 1640 medium or RPMI 1640 (Dutch modified) (Life Technologies-Invitrogen) supplemented with 10% FBS from Greiner Bio-One, Alphen a/d Rijn, The Netherlands and 2 mM L-alanyl-L-glutamine (GlutaMAX) (PAA, Linz, Austria), 100 U/ml penicillin and 100 µg/ml streptomycin (both Life Technologies-Invitrogen) (complete RPMI). Macrophages were harvested using Trypsin-EDTA 0.05% (ThermoFisher Scientific) and scraping. Macrophage differentiation was evaluated by quantification of IL-10 and IL-12p40 secretion using ELISA in the presence or absence of 24-hour stimulation with 100 ng/ml of lipopolysaccharide (LPS; InvivoGen, San Diego, United States).

Zebrafish culture

Zebrafish were maintained and handled in compliance with the local animal welfare regulations as overseen by the Animal Welfare Body of Leiden University (license number: 10612). All practices involving zebrafish were performed in accordance with European laws, guidelines and policies for animal experimentation, housing, and care (European Directive 2010/63/EU on the protection of animals used for scientific purposes). The present study did not involve any procedures within the meaning of Article 3 of Directive 2010/63/EU and as such is not subject to authorization by an ethics committee. Zebrafish lines (Supplementary Table S1) were maintained according to standard protocols (www.zfin.org). Zebrafish eggs were obtained by natural spawning of single crosses to achieve synchronized developmental timing. Eggs from at least 5 couples were combined to achieve heterogeneous groups. Eggs and embryos were kept in egg water (60 µg/ml sea salt, Sera Marin, Heinsberg, Germany) at ~28.5 °C after harvesting and in embryo medium after infection and/or treatment (E2, buffered medium, composition: 15 mM NaCl, 0.5mM KCl, 1 mM MgSO¬4, 150 µM KH2PO4, 1 mM CaCl2 and 0.7 mM NaHCO3) at ~28.5 °C for the duration of experiments.

Zebrafish genotyping

Larvae obtained by incrossing heterozygous *esr2b* mutants (*esr2b*$^{+/-}$) zebrafish were genotyped at the end point of infection experiments. Larvae were collected individually in 100 µl of 50 mM NaOH. Samples were heated to 95 °C for 10 min until the larvae dissolved, cooled to 4 °C and then 10 µl of 1 M Tris, pH 7.5, was added to neutralize the basic solution and centrifuged to pull down any tissue debris, essentially as described [78]. Supernatant was directly used for PCR amplification of the genetic region of interest followed by Sanger sequencing to identify the genotype (BaseClear, Netherlands). Sequences of the primers are provided in Supplementary Table S1.

Bacterial cultures

Mtb (H37Rv), DsRed-expressing H37Rv, mWasabi-or mCherry- expressing *Mm* M-strain[79,80] were cultured in Difco Middlebrook 7H9 broth (Becton Dickinson, Breda, the Netherlands) supplemented with 10% ADC (Becton Dickinson), 0.05% Tween 80 (Sigma-Aldrich) and 50 µg/ml Hygromycin B (Life Technologies-Invitrogen). *Stm* strain SL1344 was cultured in Difco lysogeny broth (LB) (Becton Dickinson). *Mtb* and *Stm* were cultured at 37°C while *Mm* was grown at ~28.5°C

Bacterial infection of human cells

Mtb and *Mm* suspensions were prepared from a running culture, which were one day prior to infection diluted to a density corresponding with early log-phase growth (optical density at 550 or 600 nm ($OD_{550/600}$) of 0.25). *Stm* was grown overnight, subsequently diluted 1:33 in fresh LB and used after approximately 3 hours of incubation, when log-phase growth was achieved (OD_{600} of 0.5). Bacteria were diluted in complete RPMI or

complete IMDM without antibiotics for infection of primary cells and MelJuSo cells, respectively, as described previously[34,35]. We consistently used a multiplicity of infection (MOI) of 10 for all *in vitro* infection experiments. Primary cells and MelJuSo cells, seeded at a density of 30,000 and 10,000 cells per well, respectively, in 96-well flat-bottom plates 1 day prior to infection, were inoculated with 100 µl of the bacterial suspension. Cells were subsequently centrifuged for 3 min at 800 rpm and incubated at 37°C/5% CO_2 for 20 min in case of *Stm* infections or 60 min in case of *Mtb* and *Mm* infections. Extracellular bacteria were then washed away with culture medium containing 30 µg/ml Gentamicin sulfate, incubated for 10 min at 37°C/5% CO2, followed by replacement with medium containing 5 µg/ml Gentamicin sulfate and, if indicated, chemical compounds until readout. MOI of the inoculum was verified by a standard colony-forming unit (CFU) assay.

Bacterial infection of zebrafish embryos

Fresh *Mm* inoculum was prepared for every infection experiment as described[81]. The final inoculum was resuspended in PBS containing 2% (w/v) polyvinylpyrrolidone (PVP40). The injection dose was determined by optical density measurement (OD_{600} of 1 corresponds to ~100 CFU/nl). Infection experiments were carried out according to previously described procedures[81]. In brief, microinjections were performed using borosilicate glass microcapillary injection needles (Harvard Apparatus, 300038, 1mm O.D. x 0.78mm I.D.) prepared using a micropipette puller device (Sutter Instruments Flaming/Brown P-97). Needles were mounted on a micromanipulator (Sutter Instruments MM-33R) positioned under a stereo microscope. Prior to injection at 30 hours post fertilization (hpf), embryos were anesthetized using 200 µg/ml buffered 3-aminobenzoid acid (Tricaine, Sigma-Aldrich) in egg water. They were then positioned on a 1% agarose plate (in egg water) and injected into the blood island with an 1 nL inoculum containing ~200 CFU *Mm*. For assessment of bacterial burden, larvae were anesthetized using tricaine at 4 days post infection (dpi), positioned on a 1% agarose (in egg water) plate and imaged using a Leica M205 FA stereo fluorescence microscope equipped with a DFC345 FX monochrome camera. Bacterial burden was determined based on fluorescent pixel quantification[82].

Chemical compound treatments

Cells were treated with chemical compound or 100% DMSO at equal v/v in medium containing 5 µg/ml gentamicin sulfate as described previously[34,35]. Treatment of zebrafish embryos was performed by immersion. Stock concentrations were diluted to treatment doses in complete IMDM or embryo medium without antibiotics, for human cells and zebrafish embryos, respectively. As a solvent control treatment, 100% DMSO was diluted to the same concentration as the compound treatment. If different tamoxifen treatment doses were used in the same zebrafish embryo experiment, the solvent control concentration corresponding to the highest tamoxifen treatment dose was used. Precise doses of compound treatments and solvent control concentrations as well as the durations of treatment are described in the figure legends for each individual experiment.

Colony-forming unit (CFU) assay

Cells were lysed in H_2O containing 0.05% SDS (ThermoFisher Scientific). Lysates of *Mtb*-infected cells were 5-fold serially diluted in 7H9 broth, and 10 µl droplets were spotted onto square Middlebrook 7H10 agar plates. Plates were incubated at 37°C for 12-14 days and bacterial colonies quantified using a microscope with a magnification of 2.5 times to enhance early detection of bacterial growth. Lysates of *Stm*-infected cells were serially diluted in 10-fold steps in LB broth, and 10 µl droplets were spotted onto

square LB agar plates and incubated overnight at 37°C.

Liquid bacterial growth assay

Stm or *Mtb* and *Mm* culture in logarithmic growth phase was diluted to an $OD_{550\ or}$ OD_{600} of 0.05 in LB broth or 0.1 in complete 7H9 broth respectively, of which 200 µl per flat-bottom 96-well was incubated with chemical compound, antibiotic or DMSO at equal v/v at indicated concentrations. *Stm* growth (OD_{550}) was measured after overnight incubation at 37°C, while *Mm* growth was evaluated during 2 days of incubation at ~28.5°C and *Mtb* growth for 10 days of incubation at 37°C.

Flow cytometry

Infected cells were at experimental endpoint washed with 100 µl of PBS and detached by incubation in 50 µl of Trypsin-EDTA 0.05% for several minutes. Single cell suspensions were fixed by adding 100 µl of 1.5% paraformaldehyde with subsequent incubation for 60 min at 4°C. Acquisition was performed using a BD FACSCalibur combined with a High Throughput Sampler (HTS) (BD BioSciences). Data were analyzed using FlowJo software v9.

Immunostaining

Cells were seeded on poly-d-lysine coated glass-bottom (no. 1.5) 96-well plates (MatTek, Ashland, Massachusetts, United States) that were pre-washed with PBS, at a density of 30,000 per well. After overnight incubation, cells were infected with DsRed-expressing *Mtb* at a MOI of 10 as described above. At the indicated experimental endpoint, cells were washed three times with PBS and fixed for 60 min at RT using 1% methanol-free EM-grade formaldehyde (ThermoFisher Scientific) diluted in PBS. Cells were washed with PBS and remaining reactive formaldehyde was quenched using 100 µl of Glycine solution (1.5 mg/ml in PBS) for 10 min at RT. Fluorescent dyes LysoTracker Deep Red (ThermoFisher Scientific) (75nM) and Cyto-ID 2.0 (Enzo LifeSciences) (1:500) were added to the cells 30 minutes prior to treatment endpoint and, after the washing and fixation procedure described above, counterstained with 50 ul of 2 µg/ml Hoechst 33342 (Sigma-Aldrich) at RT in the dark. For staining using antibodies, cells were permeabilized in 0.1% Triton-X (Sigma-Aldrich) diluted in PBS for 10 min at RT and Fc-receptors were subsequently blocked using 5% human serum (HS; Sanquin Blood bank, Amsterdam, The Netherlands) for 45 min at RT. After removal of the 5% HS, cells were stained with 50 ul of primary antibody diluted in 5% HS for 30 min at RT, washed three times with 5% HS and incubated with 50 ul of secondary antibody in 5% HS for 30 min at RT in the dark. After washing three times with 5% HS, cells were counterstained with Hoechst 33342 and Phalloidin as described above. Images, at least 3 per well, were acquired using a Leica TCS SP8 X WLL confocal system and 63X oil immersion objective. Hybrid detectors were used with a time gate to switch off data collection during the pulse.

Colocalization analysis of *Mtb*-infected cells was performed as follows. Image background was subtracted using the rolling ball (20-pixel radius) algorithm with Fiji software version 1.53c[83]. CellProfiler 3.0.0[84] was used to first correct for non-homogenous illumination if necessary, then for the segmentation of both the fluorescent bacteria and marker of interest using global thresholding with intensity-based declumping[84]. For every experiment, segmentation was performed with both a range of thresholds and adaptive three-class Otsu thresholding independently to confirm segmentation results. Then per image the overlap of *Mtb* with marker of interest was calculated as percentage of object overlap. To avoid potentially confounding results, two donors were excluded from colocalization results (Figures 4A and 5B) due to extensive intensity background

levels in treated samples.

GFP-Lc3 and LysoTracker imaging in zebrafish larvae

For visualization of Lc3 dynamics, Tg(CMV:EGFP-map1lc3b) larvae were embedded in 1.5% low melting point agarose (weight per volume, in egg water) and imaged using a Leica TCS SPE confocal microscope. Imaging was performed using a 63x oil immersion objective (HC PL APO CS2, NA 1.42) in a region of the tail fin to detect EGFP-map1lc3b – further referred as GFP-Lc3 – positive vesicles. For quantification of acidic vesicles in presence and absence of infection, larvae were immersed in embryo medium containing 5 µM LysoTracker Red DND-99 solution (ThermoFisher Scientific) for 1 hour. Before mounting and imaging, larvae were washed 3 times with embryo medium. To determine colocalization between *Mm* and GFP-Lc3 or LysoTracker, fixed (GFP-Lc3) or live anesthetized (LysoTracker) larvae were embedded in 1.5% low melting agarose (in egg water) and imaged in the caudal hematopoietic tissue, using a Leica TCS SP8 confocal microscope with a 40x water immersion objective (HCX APO L U-V-I, NA 0.8). Images were obtained using Leica Las X software. For the quantification of GFP-Lc3 levels the find maxima algorithm with a noise tolerance of 50 was used in Fiji software version 1.53c. To determine association of GFP-Lc3 or LysoTracker with bacteria, manual counting was performed on the obtained confocal images using Leica Las X software.

Tail amputation of zebrafish larvae

Embryos of an Tg(mpeg1:mcherryF)/Tg(mpx;gfp) double transgenic line were anesthetized using tricaine at 3 days post fertilization (dpf), positioned on a 1% agarose (in egg water) plate and the tails were partially amputated with a 1 mm sapphire blade (World Precision Instruments) under a Leica M165C stereomicroscope[85]. After amputation larvae were incubated in embryo medium for 4 hours and fixed using 4% paraformaldehyde. After fixation, larvae were positioned on a 1% agarose (in egg water) plate and imaged using a Leica M205 FA stereofluorescence microscope equipped with a DFC345 FX monochrome camera. Macrophages were detected based on the fluorescence of their mCherry label and neutrophils were detected based on their GFP label. The number of leukocytes recruited to the wounded area were counted as described previously[85].

RNA isolation, cDNA synthesis and qPCR

Zebrafish larvae (10 per sample) were collected at the experimental endpoint in QIAzol lysis reagent (Qiagen, Hilden, Germany). RNA was isolated using miRNeasy mini kit (Qiagen, Hilden, Germany) according to the manufacturer's instructions and the iScript cDNA Synthesis Kit (BioRad, Hercules, US) was used for reverse-transcription of the extracted total RNA. Quantitative RT-PCR (qPCR) was performed on a BioRad CFX96 machine following a two-step protocol with 40 cycles with a 95 °C melting temperature for 15s and 60 °C annealing and amplification for 30s. All reactions on the 3 biological replicates (3 samples/treatment group) were performed with 3 technical replicates (3 wells/sample). Analysis of qPCR results was performed using the ΔΔCt method and data were normalized to the expression of the housekeeping gene *tbp* (TATA box binding protein). Two ER-target genes were analyzed: *cyp19a1b* (cytochrome P450, family 19, subfamily A, polypeptide 1a) and *vtg1* (vitellogenin 1). Sequences of the primers are provided in Supplementary Table S1.

RNA sequencing and data analysis

Tamoxifen treatment of zebrafish larvae was performed from 1 hour post infection (hpi) until 2 dpi (3 dpf). Next, larvae were collected (10 per sample) for RNA isolation as described above. RNA integrity was assessed by Bioanalyzer (Agilent, Santa Clara, US)

and all samples were found to have a RIN ≥ 9.5. Of the total RNA, 3µg was used to create RNAseq libraries using the Illumina TruSeq strand-specific mRNA polyA preparation kit (Illumina, San Diego, US). The resulting RNAseq library was sequenced for at least 10 million reads per sample using an Illumina HiSeq2500 with a read length of 1 × 50 nucleotides (Baseclear, Leiden, The Netherlands). Four biological replicates for each treatment and infection regime were sequenced and mapped and quantified against the *D. rerio* GRCzv11 using Salmon v0.14.1[86]. Downstream analysis of the quantified libraries was performed in RStudio 1.2.5001[87] running R 3.6.1[88]. Libraries were imported using tximport v.1.12.3[89]. Differential gene expression was assessed via pairwise comparisons using DESeq2 v1.24.0[90] following a linear model taking into account possible gene expression differences from the embryo parents, drug treatments, infections, and its interaction (design: ~genotype + treatment + infection + treatment:infection). Statistical significance was defined by s-value ≤ 0.005 using apeglm[91]. S-values are aggregate statistics that have been recently proposed as an alternative to adjusted *p*-value and false discovery rate (FDR), calculating the probability of getting the sign of an effect wrong in biological contexts[92].

Venn Diagram and enrichment analysis, including pathway and GO analysis as well as Gene Set Enrichment Analysis with the C2 "Curated Gene Sets" and C5 "GO Gene Sets" collections from the Molecular Signatures Database (MSigDB) were performed as previously described[43]. Raw data are deposited into the Gene Expression Omnibus under accession number GSE178919. The data and code to recapitulate all figures and findings in this manuscript are available at https://github.com/gabrifc/rnaseq-tamox-amio.

Data analysis and statistics

The unpaired T test or One-way ANOVA with Dunnett's or Hold-Sidak's multiple comparison test was applied when assessing differences between 2 or more groups, respectively, of unpaired data representing technical replicates. Mann-Whitney U test was applied for testing differences between unpaired data representing biological replicates. When assessing differences between 2 or more groups with paired observations of biological replicates, the Wilcoxon matched-pairs signed rank test was used, except for data that was normally distributed according to the Shapiro-Wilk test, which was assessed using a paired T test. Two-way ANOVA with Dunnett's or Tukey's multiple comparison test was used when the effect of two independent variables was tested simultaneously to either a control mean or every other mean of data representing technical replicates, respectively. Data were normalized to the mean of the control group and independent repeats were combined , unless otherwise indicated. The number of experiments combined is indicated in the figure legend for each experiment. With exception of the transcriptome profiling analysis, all analyses were performed using GraphPad Prism 8 and the statistical test performed for each experiment is described in the figure legend. Dot plot graphs of zebrafish experiments were made using the raincloud plots application at https://gabrifc.shinyapps.io/raincloudplots/[93].

Acknowledgements

We gratefully acknowledge Dr J. Bestebroer (VUMC, Amsterdam, The Netherlands) for mycobacterial reporter constructs, Dick van Soolingen and Kirsten Kremer (RIVM, Bilthoven, The Netherlands) for providing the MDR-*Mtb* strains, and Victor Mulero (University of Murcia) for the zebrafish *esr2b* mutant.

This project was funded by NWO Domain Applied and Engineering Sciences (NWO-TTW grant 13259), the Netherlands Organization for Health Research and Development (ZonMw-TOP grant 91214038), the European Union's Seventh Programme for research, technological development and demonstration under grant agreement N° PhagoSys HEALTH-F4-2008-223451, and the Horizon2020 European Marie Skłodowska-Curie programme (fellowship H2020-COFUND-2015-FP-707404). We acknowledge the support from FAPESP (grant: 2017/03332-5) to CS fellowship. The funders had no role in study design, data collection and analysis, decision to publish, or preparation of the manuscript. The authors declare that they have no conflicting interests.

References

1. Houben, R. M. G. J. & Dodd, P. J. The Global Burden of Latent Tuberculosis Infection: A Re-estimation Using Mathematical Modelling. *Plos Med* **13**, doi:ARTN e1002152, 10.1371/journal.pmed.1002152 (2016).

2. WHO. Global Tuberculosis Report 2020. *World Health Organization* (2020).

3. Davenne, T. & McShane, H. Why don't we have an effective tuberculosis vaccine yet? *Expert Rev Vaccines* **15**, 1009-1013, doi:10.1586/14760584.2016.1170599 (2016).

4. Diacon, A. H. *et al.* Randomized pilot trial of eight weeks of bedaquiline (TMC207) treatment for multidrug-resistant tuberculosis: long-term outcome, tolerability, and effect on emergence of drug resistance. *Antimicrob Agents Chemother* **56**, 3271-3276, doi:10.1128/AAC.06126-11 (2012).

5. Gler, M. T. *et al.* Delamanid for multidrug-resistant pulmonary tuberculosis. *N Engl J Med* **366**, 2151-2160, doi:10.1056/NEJMoa1112433 (2012).

6. Lee, M. *et al.* Linezolid for treatment of chronic extensively drug-resistant tuberculosis. *N Engl J Med* **367**, 1508-1518, doi:10.1056/NEJMoa1201964 (2012).

7. Keam, S. J. Pretomanid: First Approval. *Drugs* **79**, 1797-1803, doi:10.1007/s40265-019-01207-9 (2019).

8. Kadura, S. *et al.* Systematic review of mutations associated with resistance to the new and repurposed Mycobacterium tuberculosis drugs bedaquiline, clofazimine, linezolid, delamanid and pretomanid. *J Antimicrob Chemother* **75**, 2031-2043, doi:10.1093/jac/dkaa136 (2020).

9. Vergne, I., Gilleron, M. & Nigou, J. Manipulation of the endocytic pathway and phagocyte functions by Mycobacterium tuberculosis lipoarabinomannan. *Front Cell Infect Microbiol* **4**, 187, doi:10.3389/fcimb.2014.00187 (2014).

10. Bussi, C. & Gutierrez, M. G. Mycobacterium tuberculosis infection of host cells in space and time. *FEMS Microbiol Rev* **43**, 341-361, doi:10.1093/femsre/fuz006 (2019).

11. Machelart, A., Song, O. R., Hoffmann, E. & Brodin, P. Host-directed therapies offer novel opportunities for the fight against tuberculosis. *Drug Discov Today* **22**, 1250-1257, doi:10.1016/j.drudis.2017.05.005 (2017).

12. Kilinc, G., Saris, A., Ottenhoff, T. H. M. & Haks, M. C. Host-directed therapy to combat mycobacterial infections*. *Immunological Reviews*, doi:10.1111/imr.12951 (2021).

13. Wallis, R. S. & Hafner, R. Advancing host-directed therapy for tuberculosis. *Nature Reviews Immunology* **15**, 255 (2015).

14. Zumla, A. *et al.* Towards host-directed therapies for tuberculosis. *Nat Rev Drug Discov* **14**, 511-512, doi:10.1038/nrd4696 (2015).

15. Hawn, T. R., Matheson, A. I., Maley, S. N. & Vandal, O. Host-directed therapeutics for tuberculosis: can we harness the host? *Microbiol Mol Biol Rev* **77**, 608-627, doi:10.1128/MMBR.00032-13 (2013).

16. Deretic, V., Saitoh, T. & Akira, S. Autophagy in infection, inflammation and immunity. *Nat Rev Immunol* **13**, 722-737, doi:10.1038/nri3532 (2013).

17. Maiuri, M. C. & Kroemer, G. Therapeutic modulation of autophagy: which disease comes first? *Cell Death Differ* **26**, 680-689, doi:10.1038/s41418-019-0290-0 (2019).

18. Keller, M. D., Torres, V. J. & Cadwell, K. Autophagy and microbial pathogenesis. *Cell Death Differ* **27**, 872-886, doi:10.1038/s41418-019-0481-8 (2020).

19. Gutierrez, M. G. *et al.* Autophagy is a defense mechanism inhibiting BCG and Mycobacterium tuberculosis survival in infected macrophages. *Cell* **119**, 753-766, doi:DOI 10.1016/j.cell.2004.11.038 (2004).

20. Bradfute, S. B. *et al.* Autophagy as an immune effector against tuberculosis. *Current Opinion in Microbiology* **16**, 355-365, doi:10.1016/j.mib.2013.05.003 (2013).

21. Tobin, D. M. Host-Directed Therapies for Tuberculosis. *Cold Spring Harb Perspect Med* **5**, doi:10.1101/cshperspect.a021196 (2015).

22. Zembutsu, H. Pharmacogenomics toward personalized tamoxifen therapy for breast cancer. *Pharmacogenomics* **16**, 287-296, doi:10.2217/pgs.14.171 (2015).

23. Gallo, M. A. & Kaufman, D. Antagonistic and agonistic effects of tamoxifen: significance in human cancer. *Semin Oncol* **24**, S1-71-S71-80 (1997).

24. Shagufta & Ahmad, I. Tamoxifen a pioneering drug: An update on the therapeutic potential of tamoxifen derivatives. *Eur J Med Chem* **143**, 515-531, doi:10.1016/j.ejmech.2017.11.056 (2018).

25. Heemskerk, M. K., CJ. Esselink, J. Carvalho dos Santos, C. van Veen, S. Gordijn, IF. Vrieling, F. Walburg, KV. Engele, CG. Dijkman, D. Wilson, L. Verreck, FAW. Ottenhoff, THM. Haks, MC. Repurposing diphenylbutylpiperidine-class antipsychotic drugs for host-directed therapy of *Mycobacterium tuberculosis* and *Salmonella enterica* infections. doi:https://doi.org/10.1101/2021.06.05.447191 (2021).

26. Miguel, D. C. *et al.* Tamoxifen as a potential antileishmanial agent: efficacy in the treatment of Leishmania braziliensis and Leishmania chagasi infections. *J Antimicrob Chemoth* **63**, 365-368, doi:10.1093/jac/dkn509 (2009).

27. Butts, A. *et al.* Estrogen receptor antagonists are anti-cryptococcal agents that directly bind EF hand proteins and synergize with fluconazole in vivo. *mBio* **5**, e00765-00713, doi:10.1128/mBio.00765-13 (2014).

28. Chen, F. C. *et al.* Pros and cons of the tuberculosis drugome approach--an empirical analysis. *PLoS One* **9**, e100829, doi:10.1371/journal.pone.0100829 (2014).

29. Jang, W. S. *et al.* Anti-Mycobacterial Activity of Tamoxifen Against Drug-Resistant and Intra-Macrophage Mycobacterium tuberculosis. *J Microbiol Biotechnol* **25**, 946-950, doi:10.4014/jmb.1412.12023 (2015).

30. Dittmar, A. J., Drozda, A. A. & Blader, I. J. Drug Repurposing Screening Identifies Novel Compounds That Effectively Inhibit Toxoplasma gondii Growth. *Msphere* **1**, doi:ARTN e00042-15, 10.1128/mSphere.00042-15 (2016).

31. Corleis, B. & Dorhoi, A. Early dynamics of innate immunity during pulmonary tuberculosis. *Immunol Lett* **221**, 56-60, doi:10.1016/j.imlet.2020.02.010 (2020).

32. Rothchild, A. C. *et al.* Alveolar macrophages generate a noncanonical NRF2-driven transcriptional response to Mycobacterium tuberculosis in vivo. *Sci Immunol* **4**, doi:10.1126/sciimmunol.aaw6693 (2019).

33. Thiriot, J. D., Martinez-Martinez, Y. B., Endsley, J. J. & Torres, A. G. Hacking the host: exploitation of macrophage polarization by intracellular bacterial pathogens. *Pathog Dis* **78**, doi:10.1093/femspd/ftaa009 (2020).

34. Korbee, C. J. *et al.* Combined chemical genetics and data-driven bioinformatics approach identifies receptor tyrosine kinase inhibitors as host-directed antimicrobials. *Nat Commun* **9**, 358, doi:10.1038/s41467-017-02777-6 (2018).

35. Moreira, J. D. *et al.* Functional Inhibition of Host Histone Deacetylases (HDACs) Enhances in vitro and in vivo Anti-mycobacterial Activity in Human Macrophages and in Zebrafish. *Frontiers in Immunology* **11**, doi:ARTN 36, 10.3389/fimmu.2020.00036 (2020).

36. Keiser, T. L. & Purdy, G. E. Killing Mycobacterium tuberculosis In Vitro: What Model Systems Can Teach Us. *Microbiology Spectrum* **5**, doi:UNSP TBTB2-0028-2016, 10.1128/microbiolspec.TBTB2-0028-2016 (2017).

37. Davis, J. M. *et al.* Real-time visualization of mycobacterium-macrophage interactions leading to initiation of granuloma formation in zebrafish embryos. *Immunity* **17**, 693-702, doi:10.1016/s1074-7613(02)00475-2 (2002).

38. Meijer, A. H. Protection and pathology in TB: learning from the zebrafish model. *Semin Immunopathol* **38**, 261-273, doi:10.1007/s00281-015-0522-4 (2016).

39. Berg, R. D. & Ramakrishnan, L. Insights into tuberculosis from the zebrafish model. *Trends Mol Med* **18**, 689-690, doi:10.1016/j.molmed.2012.10.002 (2012).

40. van der Vaart, M. *et al.* The DNA damage-regulated autophagy modulator DRAM1 links mycobacterial recognition via TLR-MYD88 to autophagic defense [corrected]. *Cell Host Microbe* **15**, 753-767, doi:10.1016/j.chom.2014.05.005 (2014).

41. Hosseini, R. *et al.* Correlative light and electron microscopy imaging of autophagy in a zebrafish infection model. *Autophagy* **10**, 1844-1857, doi:10.4161/auto.29992 (2014).

42. Zhang, R. *et al.* The selective autophagy receptors Optineurin and p62 are both required for zebrafish host resistance to mycobacterial infection. *Plos Pathog* **15**, doi:ARTN e1007329, 10.1371/journal.ppat.1007329 (2019).

43. Zhang, R. *et al.* Deficiency in the autophagy modulator Dram1 exacerbates pyroptotic cell death of Mycobacteria-infected macrophages. *Cell Death Dis* **11**, 277, doi:10.1038/s41419-020-2477-1 (2020).

44. Verreck, F. A. W., de Boer, T., Langenberg, D. M. L., van der Zanden, L. & Ottenhoff, T. H. M. Phenotypic and functional profiling of human proinflammatory type-1 and anti-inflammatory type-2 macrophages in response to microbial antigens and IFN-gamma- and CD40L-mediated costimulation. *Journal of Leukocyte Biology* **79**, 285-293, doi:10.1189/jlb.0105015 (2006).

45. Verreck, F. A. *et al.* Human IL-23-producing type 1 macrophages promote but IL-10-producing type 2 macrophages subvert immunity to (myco)bacteria. *Proc Natl Acad Sci U S A* **101**, 4560-4565, doi:10.1073/pnas.0400983101 (2004).

46. Benard, E. L., Rougeot, J., Racz, P. I., Spaink, H. P. & Meijer, A. H. Transcriptomic Approaches in the Zebrafish Model for Tuberculosis-Insights Into Host- and Pathogen-specific Determinants of the Innate Immune Response. *Adv Genet* **95**, 217-251, doi:10.1016/bs.adgen.2016.04.004 (2016).

47. Cardoso, C. M., Custodio, J. B., Almeida, L. M. & Moreno, A. J. Mechanisms of the deleterious effects of tamoxifen on mitochondrial respiration rate and phosphorylation efficiency. *Toxicol Appl Pharmacol* **176**, 145-152, doi:10.1006/taap.2001.9265 (2001).

48. Nazarewicz, R. R. *et al.* Tamoxifen induces oxidative stress and mitochondrial apoptosis via stimulating mitochondrial nitric oxide synthase. *Cancer Res* **67**, 1282-1290, doi:10.1158/0008-5472.CAN-06-3099 (2007).

49. Pattingre, S., Bauvy, C., Levade, T., Levine, B. & Codogno, P. Ceramide-induced autophagy: to junk or to protect cells? *Autophagy* **5**, 558-560, doi:10.4161/auto.5.4.8390 (2009).

50. Davis, J. M. & Ramakrishnan, L. The role of the granuloma in expansion and dissemination of early tuberculous infection. *Cell* **136**, 37-49, doi:10.1016/j.cell.2008.11.014 (2009).

51. Yang, C. T. *et al.* Neutrophils exert protection in the early tuberculous granuloma by oxidative killing of mycobacteria phagocytosed from infected macrophages. *Cell Host Microbe* **12**, 301-312, doi:10.1016/j.chom.2012.07.009 (2012).

52. Torraca, V. *et al.* The CXCR3-CXCL11 signaling axis mediates macrophage recruitment and dissemination of mycobacterial infection. *Dis Model Mech* **8**, 253-269, doi:10.1242/dmm.017756 (2015).

53. Corriden, R. *et al.* Tamoxifen augments the innate immune function of neutrophils through modulation of intracellular ceramide. *Nat Commun* **6**, 8369, doi:10.1038/ncomms9369 (2015).

54. Ligeiro de Oliveira, A. P., Oliveira-Filho, R. M., da Silva, Z. L., Borelli, P. & Tavares de Lima, W. Regulation of allergic lung inflammation in rats: interaction between estradiol and corticosterone. *Neuroimmunomodulation* **11**, 20-27, doi:10.1159/000072965 (2004).

55. Moreland, J. G., Davis, A. P., Bailey, G., Nauseef, W. M. & Lamb, F. S. Anion channels, including ClC-3, are required for normal neutrophil oxidative function, phagocytosis, and transendothelial migration. *J Biol Chem* **281**, 12277-12288, doi:10.1074/jbc.M511030200 (2006).

56. Xie, Y., Meijer, A. H. & Schaaf, M. J. M. Modeling Inflammation in Zebrafish for the Development of Anti-inflammatory Drugs. *Front Cell Dev Biol* **8**, 620984, doi:10.3389/fcell.2020.620984 (2020).

57. Dluzen, D. E. & Mickley, K. R. Gender differences in modulatory effects of tamoxifen upon the nigrostriatal dopaminergic system. *Pharmacol Biochem Be* **80**, 27-33, doi:10.1016/j.pbb.2004.10.007 (2005).

58. Campesi, I., Marino, M., Montella, A., Pais, S. & Franconi, F. Sex Differences in Estrogen Receptor alpha and beta Levels and Activation Status in LPS-Stimulated Human Macrophages. *J Cell Physiol* **232**, 340-345, doi:10.1002/jcp.25425 (2017).

59. Subramanian, A. *et al.* Gene set enrichment analysis: a knowledge-based approach for interpreting genome-wide expression profiles. *Proc Natl Acad Sci U S A* **102**, 15545-15550, doi:10.1073/pnas.0506580102 (2005).

60. Menuet, A. *et al.* Molecular characterization of three estrogen receptor forms in zebrafish: binding characteristics, transactivation properties, and tissue distributions. *Biol Reprod* **66**, 1881-1892, doi:10.1095/biolreprod66.6.1881 (2002).

61. Griffin, L. B., January, K. E., Ho, K. W., Cotter, K. A. & Callard, G. V. Morpholino-mediated knockdown of ERalpha, ERbetaa, and ERbetab mRNAs in zebrafish (Danio rerio) embryos reveals differential regulation of estrogen-inducible genes. *Endocrinology* **154**, 4158-4169, doi:10.1210/en.2013-1446 (2013).

62. Lopez-Munoz, A. *et al.* Estrogen receptor 2b deficiency impairs the antiviral response of zebrafish. *Dev Comp Immunol* **53**, 55-62, doi:10.1016/j.dci.2015.06.008 (2015).

63. Nagelkerke, A., Bussink, J., Sweep, F. C. G. J. & Span, P. N. The unfolded protein response as a target for cancer therapy. *Bba-Rev Cancer* **1846**, 277-284, doi:10.1016/j.bbcan.2014.07.006 (2014).

64. He, C., Bartholomew, C. R., Zhou, W. & Klionsky, D. J. Assaying autophagic activity in transgenic GFP-Lc3 and GFP-Gabarap zebrafish embryos. *Autophagy* **5**, 520-526, doi:10.4161/auto.5.4.7768 (2009).

65. Ouyang, Q. *et al.* Bazedoxifene Suppresses Intracellular Mycobacterium tuberculosis Growth by Enhancing Autophagy. *Msphere* **5**, doi:10.1128/mSphere.00124-20 (2020).

66. Miro-Canturri, A. *et al.* Potential Tamoxifen Repurposing to Combat Infections by Multidrug-Resistant Gram-Negative Bacilli. *Pharmaceuticals (Basel)* **14**, doi:10.3390/ph14060507 (2021).

67. Hao, R. *et al.* Identification of estrogen target genes during zebrafish embryonic development through transcriptomic analysis. *PLoS One* **8**, e79020, doi:10.1371/journal.pone.0079020 (2013).

68. Vosges, M. *et al.* 17alpha-Ethinylestradiol and nonylphenol affect the development of forebrain GnRH neurons through an estrogen receptors-dependent pathway. *Reprod Toxicol* **33**, 198-204, doi:10.1016/j.reprotox.2011.04.005 (2012).

69. Wang, J. *et al.* Glucocorticoids Suppress Antimicrobial Autophagy and Nitric Oxide Production and Facilitate Mycobacterial Survival in Macrophages. *Sci Rep* **7**, 982, doi:10.1038/s41598-017-01174-9 (2017).

70. Yang, C. S. *et al.* The AMPK-PPARGC1A pathway is required for antimicrobial host defense through activation of autophagy. *Autophagy* **10**, 785-802, doi:10.4161/auto.28072 (2014).

71. Oeste, C. L., Seco, E., Patton, W. F., Boya, P. & Perez-Sala, D. Interactions between autophagic and endo-lysosomal markers in endothelial cells. *Histochem Cell Biol* **139**, 659-670, doi:10.1007/s00418-012-1057-6 (2013).

72. Ponpuak, M. *et al.* Delivery of cytosolic components by autophagic adaptor protein p62 endows autophagosomes with unique antimicrobial properties. *Immunity* **32**, 329-341, doi:10.1016/j.immuni.2010.02.009 (2010).

73. Alonso, S., Pethe, K., Russell, D. G. & Purdy, G. E. Lysosomal killing of Mycobacterium mediated by ubiquitin-derived peptides is enhanced by autophagy. *P Natl Acad Sci USA* **104**, 6031-6036, doi:10.1073/pnas.0700036104 (2007).

74. Altan, N., Chen, Y., Schindler, M. & Simon, S. M. Tamoxifen inhibits acidification in cells independent of the estrogen receptor. *P Natl Acad Sci USA* **96**, 4432-4437, doi:DOI 10.1073/pnas.96.8.4432 (1999).

75. Chen, Y., Schindler, M. & Simon, S. M. A mechanism for tamoxifen-mediated inhibition of acidification. *Journal of Biological Chemistry* **274**, 18364-18373, doi:DOI 10.1074/jbc.274.26.18364 (1999).

76. Lu, S. Y., Sung, T., Lin, N. W., Abraham, R. T. & Jessen, B. A. Lysosomal adaptation: How cells respond to lysosomotropic compounds. *Plos One* **12**, doi:ARTN e0173771, 10.1371/journal.pone.0173771 (2017).

77. Corriden, R. *et al.* Tamoxifen augments the innate immune function of neutrophils through modulation of intracellular ceramide. *Nature Communications* **6**, doi:ARTN 8369, 10.1038/ncomms9369 (2015).

78. Meeker, N. D., Hutchinson, S. A., Ho, L. & Trede, N. S. Method for isolation of PCR-ready genomic DNA from zebrafish tissues. *Biotechniques* **43**, 610, 612, 614, doi:10.2144/000112619 (2007).

79. van der Sar, A. M. *et al.* Mycobacterium marinum strains can be divided into two distinct types based on genetic diversity and virulence. *Infect Immun* **72**, 6306-6312, doi:10.1128/IAI.72.11.6306-6312.2004 (2004).

80. Takaki, K., Davis, J. M., Winglee, K. & Ramakrishnan, L. Evaluation of the pathogenesis and treatment of Mycobacterium marinum infection in zebrafish. *Nat Protoc* **8**, 1114-1124, doi:10.1038/nprot.2013.068 (2013).

81. Benard, E. L. *et al.* Infection of zebrafish embryos with intracellular bacterial pathogens. *J Vis Exp*, doi:10.3791/3781 (2012).

82. Stoop, E. J. M. *et al.* Zebrafish embryo screen for mycobacterial genes involved in the initiation of granuloma formation reveals a newly identified ESX-1 component. *Dis Model Mech* **4**, 526-536, doi:10.1242/dmm.006676 (2011).

83. Schindelin, J. *et al.* Fiji: an open-source platform for biological-image analysis. *Nat Methods* **9**, 676-682, doi:10.1038/nmeth.2019 (2012).

84. McQuin, C. *et al.* CellProfiler 3.0: Next-generation image processing for biology. *PLoS Biol* **16**, e2005970, doi:10.1371/journal.pbio.2005970 (2018).

85. Xie, Y. *et al.* Glucocorticoids inhibit macrophage differentiation towards a pro-inflammatory phenotype upon wounding without affecting their migration. *Dis Model Mech* **12**, doi:10.1242/dmm.037887 (2019).

86. Patro, R., Duggal, G., Love, M. I., Irizarry, R. A. & Kingsford, C. Salmon provides fast and bias-aware quantification of transcript expression. *Nature Methods* **14**, 417-419, doi:10.1038/nmeth.4197 (2017).

87. RStudio: Integrated Development for R. RStudio, PBC, Boston, MA (2020).

88. R: A language and environment for statistical computing. R Foundation for Statistical Computing, Vienna, Austria (2018).

89. Soneson, C., Love, M. & Robinson, M. Differential analyses for RNA-seq: transcript-level estimates improve gene-level inferences [version 2; peer review: 2 approved]. *F1000Research* **4:1521** (2016).

90. Love, M. I., Huber, W. & Anders, S. Moderated estimation of fold change and dispersion for RNA-seq data with DESeq2. *Genome Biol* **15**, 550, doi:10.1186/s13059-014-0550-8 (2014).

91. Zhu, A., Ibrahim, J. G. & Love, M. I. Heavy-tailed prior distributions for sequence count data: removing the noise and preserving large differences. *Bioinformatics* **35**, 2084-2092, doi:10.1093/bioinformatics/bty895 (2019).

92. Stephens, M. False discovery rates: a new deal. *Biostatistics* **18**, 275-294, doi:10.1093/biostatistics/kxw041 (2017).

93. Allen, M. A.-O., Poggiali, D. A.-O., Whitaker, K. A.-O., Marshall, T. R. & Kievit, R. A.-O. Raincloud plots: a multi-platform tool for robust data visualization. *Wellcome Open Res* **4:63** (2019).

Supplementary data, figures and tables

Supplementary Data File 1 can be downloaded via
https://doi.org/10.5281/zenodo.5788543

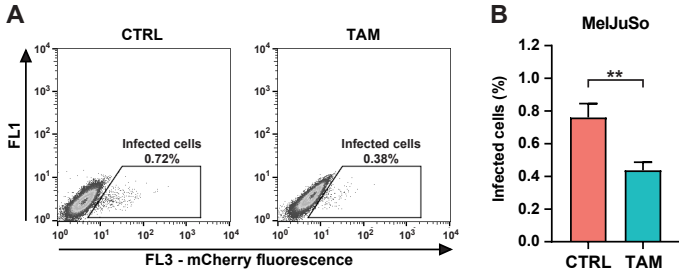

Supplementary Figure 1. Tamoxifen inhibits *Mm* burden in an *in vitro* infection model

A. Flow cytometric dot-plots of mCherry-expressing *Mm*-infected MelJuSo cells treated with 10 µM of Tamoxifen or control (DMSO at equal v/v) for 24 hours. Dot plots consist of 3 concatenated replicates and the experiment shown is a representative of 2 independent experiments.

B. Quantification of infected population shown in A. Each bar depicts the mean with standard deviation of 3 replicates. Statistical significance was tested an unpaired T test.
(** = p<0.01).

Supplementary Figure 2. Processing and quality control of zebrafish RNA sequencing data (figure on next page)

A. Principal component analysis (PCA) of transcriptomes of non-infected and *Mm*-infected zebrafish larvae treated with 5 µM of Tamoxifen or control (DMSO at equal v/v). Treatment was started at 1 hpi and isolation of RNA for RNA sequencing was performed at 2 dpi. Clustering of the different samples was driven by parent-pairs, over treatment or infection. Groups A-D indicate parent-pairs, each dot indicates a sample. Based on this result, we added the variable genotype to reflect that the major differences between samples are driven by parent-pairs in our analysis.

B. P-value histogram of the differential expression analysis of zebrafish larvae treated with 5 µM of Tamoxifen compared to treatment with control (DMSO at equal v/v), as in A. Histogram shape, which before adjusting for false discovery rates reveals test performance, showed a hill-shaped as opposed to a uniform distribution implying that the data does not fit the test assumption.

C. Volcano plot of the differential expression analysis of zebrafish larvae treated with 5 µM compared of Tamoxifen to treatment with control (DMSO at equal v/v), as in A. Red dots indicate significantly regulated genes (FDR-adjusted p-value (p.adj) ≤ 0.05), while black dots indicate non-significantly regulated genes. The subset of genes in the wings of the plot have low read counts, high inter-sample variation, and high calculated fold changes. Further analysis determined these genes as artifacts.

D. Volcano plot of the differential expression analysis as in C using apeglm to reduce variance for genes with little information while preserving large differences. The more conservative analysis method apeglm shrinks the fold-change to 0 for genes that contain insufficient information to accurately predict their fold-change. The genes with a fold change of 0 form a vertical line. Red dots indicate significantly regulated genes (p.adj) ≤ 0.05), while black dots indicate non-significantly regulated genes.

E. Volcano plot of the differential expression analysis as in D using s-values. Red dots indicate significantly regulated genes (s-value ≤ 0.005), while black dots indicate non-significantly regulated genes. By using s-values as opposed to FDR-adjusted p-values, the wings as depicted in C or vertical line as depicted in D are no longer present. Based on their s-values, these subsets of genes are deemed artifacts.

F. Correlation of transcriptome data analyzed using FDR-corrected p-values (as in D) compared to s-values (as in E). Each dot indicates a gene, the dashed lines indicate significance cut-offs. In the top left, there is a cluster of genes with low, significant adjusted p-value but high, non-significant s-value.

G. Zoom of area boxed in F, indicating the genes that are significant by both p-value (p.adj ≤ 0.05) and s-value (s ≤ 0.005).

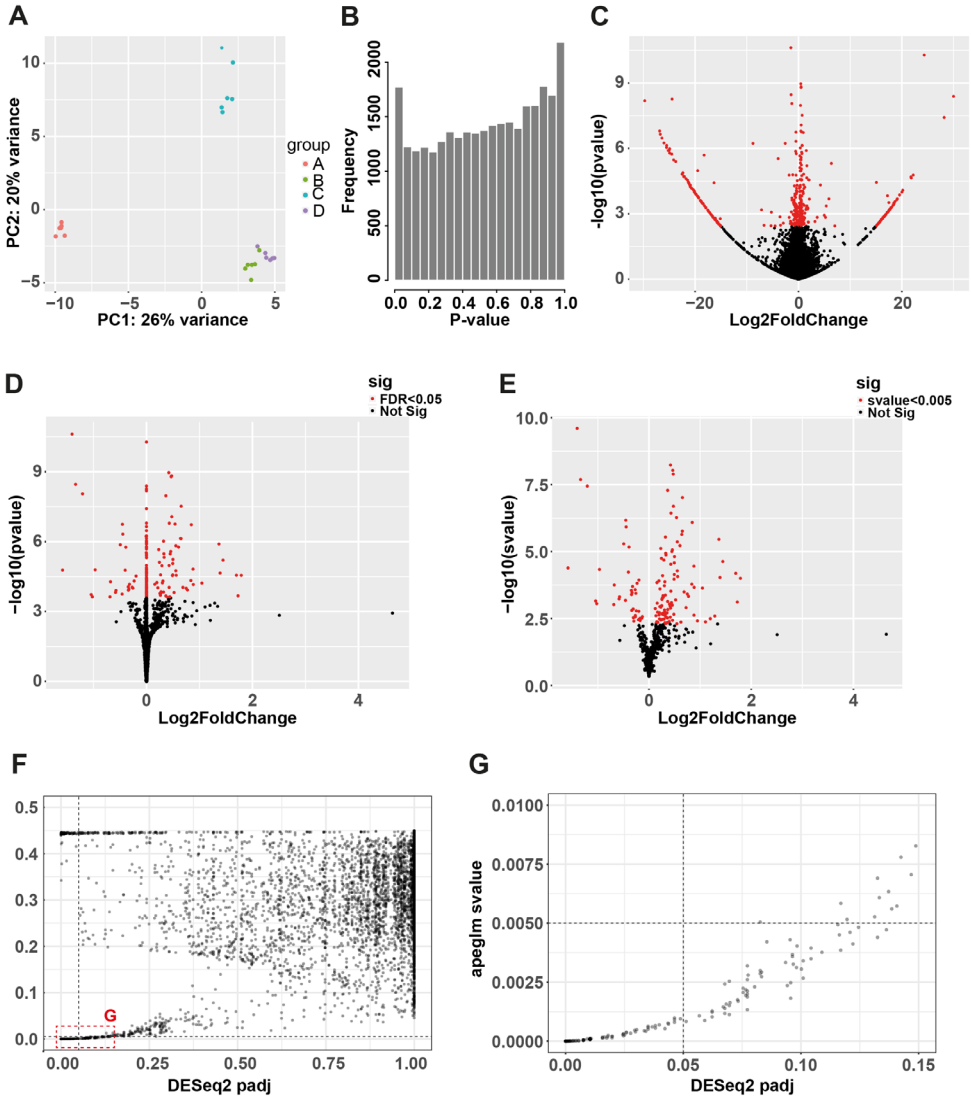
A
PC2: 20% variance
PC1: 26% variance
group
A
B
C
D
B
Frequency
P-value
C
-log10(pvalue)
Log2FoldChange
D
sig
FDR<0.05
Not Sig
-log10(pvalue)
Log2FoldChange
E
sig
svalue<0.005
Not Sig
-log10(svalue)
Log2FoldChange
F
G
DESeq2 padj
G
apeglm svalue
DESeq2 padj

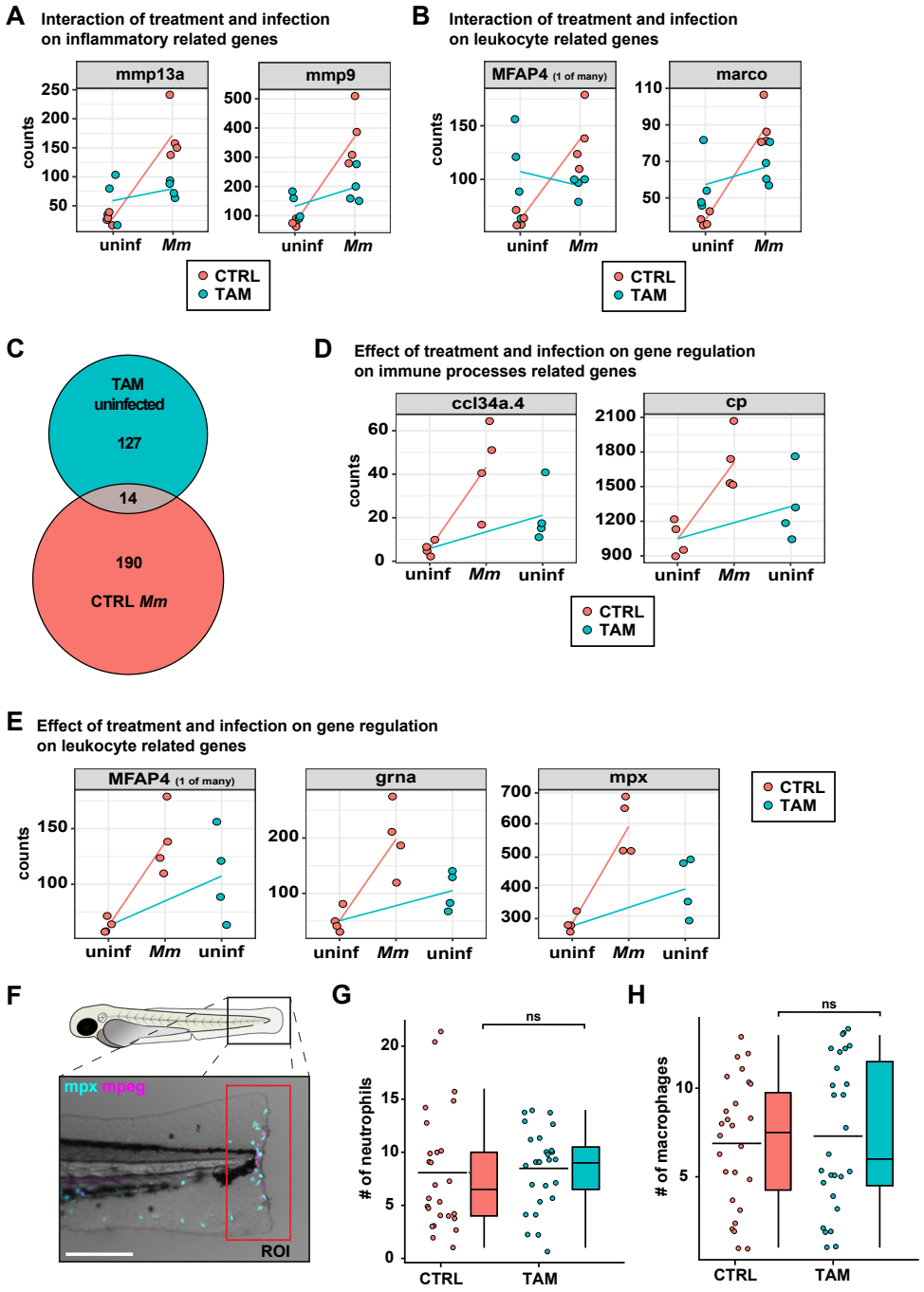

Supplementary Figure 3. Tamoxifen alters leukocyte-specific gene expression without affecting macrophage or neutrophil migration *in vivo*

Figure legend continues on next page

Supplementary Figure 3. (continued)

A-B. Interaction between Tamoxifen treatment and infection in genes that are differentially regulated (s-value ≤ 0.005, as in supplementary Figure 2E) and whose expression during infection was found to be dependent on Tamoxifen treatment. Panel A shows genes related to inflammation and B shows genes related to leukocyte function. Each dot represents the normalized gene read count of a single biological replicate (n = 10 larvae), while the line connects the means.

C. Venn diagram showing the total number of genes differentially regulated by Tamoxifen treatment in the absence of infection and by *Mm* infection in the absence of Tamoxifen treatment.

D-E. Normalized gene read counts of genes whose expression was regulated by both Tamoxifen treatment and *Mm* infection individually. D shows genes related to immune function and E shows genes related to leukocyte function. Each dot represents the normalized gene read count of a single group of larvae (n = 10), while the line connects the means.

F. Leukocyte migration assay of mpeg1:mcherryF/mpx;GFP double transgenic zebrafish larvae treated with 5 µM of Tamoxifen or control (DMSO at equal v/v). Treatment was started at 1 dpf and larvae were anesthetized and leukocyte migration was induced by tail amputation at 3 dpf. Representative stereo fluorescence images of leukocyte migration towards the injury (4 hours post amputation) are shown. Cyan shows neutrophils (*mpx*:GFP) and magenta shows macrophages (*mpeg1*:mCherryF). The region of interest (ROI) indicates the area for quantification of leukocyte migration. Scale bar annotates 220 µm.

G-H. Quantification of F, showing the number of migrated neutrophils (G) or macrophages (H). Each dot represents a single larva. Boxplots with 95% confidence intervals are shown and the black line in the boxplots indicates the group median, while the black line in the dot plot indicates the group mean. Statistical analysis was performed using a Mann-Whitney test.

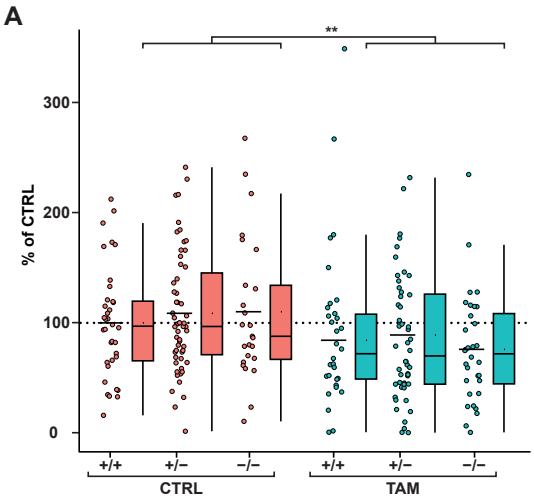

Supplementary Figure 4. The host-directed effect of Tamoxifen is independent of ER-receptor presence

A. Bacterial burden assay of mWasabi-expressing *Mm*-infected *esr2b*$^{+/+}$, *esr2b*$^{+/-}$ and *esr2b*$^{-/-}$ zebrafish larvae treated with 5 µM of Tamoxifen or control (DMSO at equal v/v). Treatment was started at 1 hpi and larvae anesthetized at 4 dpi for imaging. Bacterial burden was normalized to the control and data of 2 experimental repeats were combined (n = 25-55 per group). Each dot represents a single larva. Boxplots with 95% confidence intervals are shown and the black line in the boxplots indicates the group median, while the black line in the dot plot indicates the group mean. Dotted line indicates mean of control treated *esr2b*$^{+/+}$ zebrafish larvae set at 100%. Statistical significance of the difference between the control and Tamoxifen-treated groups was determined using a two-way ANOVA.
(** = p<0.01).

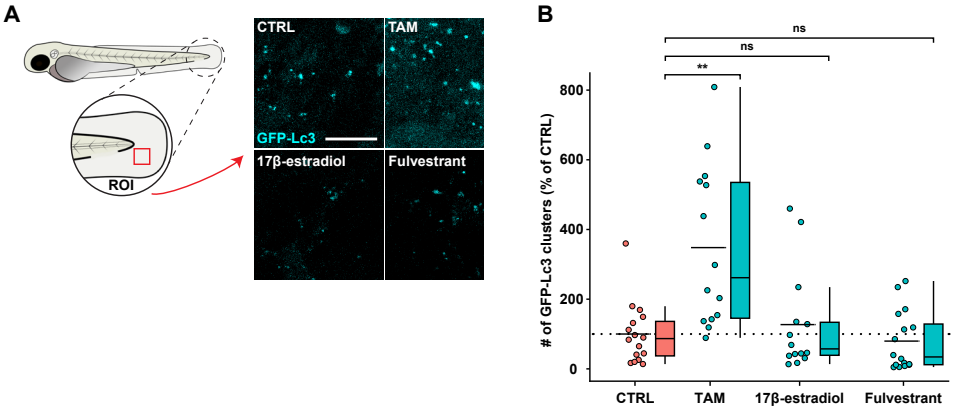

Supplementary Figure 5. Autophagy is not modulated by ER ligands in zebrafish

A. Confocal microscopy of transgenic GFP-Lc3 zebrafish larvae treated with 5 μM of Tamoxifen, 5 μM of ER agonist 17β-estradiol, 5 μM of ER antagonist Fulvestrant or control (DMSO at v/v). Treatment was started at 3 dpf and larvae were fixed with 4% paraformaldehyde at 4 dpf. Representative images of GFP-Lc3 positive vesicles in the tail fin are shown. Cyan shows GFP-Lc3 positive vesicles. Scale bar annotates 10 μm.

B. Quantification of GFP-Lc3 signal in A. Data were normalized to the control and data of 2 experimental repeats were combined (n = 14-16 per group). Each dot represents a single larva. Boxplots with 95% confidence intervals are shown and the black line in the boxplots indicates the group median, while the black line in the dot plot indicates the group mean. Dotted line indicates control mean. Statistical analysis was performed using a Kruskal-Wallis with Dunn's multiple comparisons test. (** = p<0.01).

Zebrafish lines		
Name	**Description**	**Reference**
AB/TL	Wild type strain	Zfin.org
esr2b^{sa77}	Loss of function *esr2b* mutant	Lopez-Munoz 2015
Tg(CMV:EGFP-map1lc3b)^{zf155}	GFP-tagged zebrafish Lc3	He 2009
Tg(mpeg1:mCherryF)^{umsF001}	Macrophage marker	Bernut 2014
Tg(mpx:EGFP)^{i114}	Neutrophil marker	Renshaw 2006
Tg(mpeg1:mCherryF, mpx:EGFP)$^{umsF001, i114}$	Macrophage and neutrophil marker	Bernut 2014, Renshaw 2006

Primer sequences				
Gene	**Type**	**Ensemble ID**	**Sequence**	
esr2b	PCR*	ENSDARG00000034181	FW	TCTTGGATGACATTAATAATCTGG
			RV	ATTCAACTGCAGTGTCTTGC
tbp	qPCR	ENSDARG00000014994	FW	CCTGCCCATTTTCAGTC
			RV	TGTTGTTGCCTCTGTTGCTC
cyp19a1b	qPCR	ENSDARG00000098360	FW	AAAGAGTTACTAATAAAGATCCACCGGTAT
			RV	TCCACAAGCTTTCCCATTTCA
vtg1	qPCR	ENSDARG00000092233	FW	ACTACCAACTGGCTGCTTAC
			RV	ACCATCGGCACAGATCTTC

Supplementary table S1. Supplementary materials

*The esr2b forward primer was also used for sequencing.

Gene name	Ensembl ID	s-value	Log2FC
AL935146.1	ENSDARG00000112812	0,003884	0,521512122
amd1	ENSDARG00000043856	0,000341	0,242002141
BX005175.1	ENSDARG00000112442	7,37E-05	-0,670979432
c3a.6	ENSDARG00000043719	0,002685	-0,545814275
c4b	ENSDARG00000038424	0,000121	-0,696489422
cnot2	ENSDARG00000061802	0,003033	-0,281112148
CT573383.1	ENSDARG00000097513	0,00213	-0,789054804
epg5	ENSDARG00000059846	0,001415	-0,438146512
FERMT3 (1 of many)	ENSDARG00000079267	0,004768	-1,181817384
gdi2	ENSDARG00000113039	0,0007	-0,294281106
hck	ENSDARG00000058647	0,000785	-0,732845923
hmcn2	ENSDARG00000079327	0,001891	-0,37352186
itgb2	ENSDARG00000016939	0,000284	-0,704094034
marco	ENSDARG00000059294	0,000603	-0,846209025
MFAP4 (1 of many)	ENSDARG00000088745	0,000214	-1,071839201
mfsd13a	ENSDARG00000112339	0,000522	-1,160824835
mmp13a	ENSDARG00000012395	7,33E-06	-1,905795573
mmp9	ENSDARG00000042816	1,95E-05	-1,589634402
musk	ENSDARG00000098764	0,001222	-0,637124638
psmc4	ENSDARG00000027099	0,000902	-0,507563082
ptpn13	ENSDARG00000103699	0,00347	-0,494978538
rasal2	ENSDARG00000036257	0,001658	-0,526200288
ric8b	ENSDARG00000005972	0,004342	-0,581914895
rmc1	ENSDARG00000029307	0,000445	-1,856523793
si:ch211-147m6.1	ENSDARG00000109648	4,43E-10	-1,378532336
si:ch211-194m7.3	ENSDARG00000074322	0,000388	-0,844262364
si:dkey-88l16.2	ENSDARG00000095137	0,002367	-2,336116068
trim63a	ENSDARG00000111657	0,001029	1,039071884

Supplementary table S2. Interaction of treatment and infection on gene regulation

Gene name	Ensembl ID	s-value (CTRL)	Log2FC (CTRL)	s-value (TAM)	Log2FC (TAM)
BX005175.1	ENSDARG00000101334	0,001093545	0,364449917	2,64E-05	0,495096771
ccl34a.4	ENSDARG00000074656	3,49E-11	2,834446032	6,52E-05	1,697390717
cfhl4	ENSDARG00000010312	0,001131535	0,218548149	0,000362287	-0,256087622
cp	ENSDARG00000090873	2,55E-13	0,687125852	0,003422273	0,257557489
ctsc	ENSDARG00000116951	9,22E-07	0,582920465	9,62E-08	0,65480504
ctss2.1	ENSDARG00000113068	3,89E-09	1,35242256	0,001239314	0,725429688
cul1a	ENSDARG00000004954	0,000260209	1,20735414	9,29E-05	1,389402743
grna	ENSDARG00000112150	1,59E-10	1,908385972	0,00237872	0,880257892
hist2h2l	ENSDARG00000019521	0,000665246	0,373924602	0,004626593	0,310629696
MFAP4 (1 of many)	ENSDARG00000112442	2,93E-07	1,031906608	0,004953604	0,545848653
mpx	ENSDARG00000109648	5,49E-13	1,058634459	0,002816962	0,417152838
si:ch211-147m6.1	ENSDARG00000105142	2,04E-46	2,342056078	8,18E-07	0,845930154
tcirg1b	ENSDARG00000006019	1,52E-08	0,548631879	0,002258719	0,284884932
tktb	ENSDARG00000088745	0,001875833	0,173521655	0,000247625	0,214566765

Supplementary table S3. Effect of treatment and infection on gene regulation

KEGG pathway		
Pathway	**Number of DR genes**	**padj**
Lysosome	16 (out of 140)	5,88E-14
Other glycan degradation	4 (out of 24)	0,00108355
Apoptosis	7 (out of 164)	0,003841255
Phagosome	6 (out of 142)	0,010176479
Glycosphingolipid biosynthesis - globo and isoglobo series	2 (out of 8)	0,028298257
Metabolic pathways	18 (out of 1286)	0,028298257
Ferroptosis	3 (out of 41)	0,048131463
Autophagy - animal	5 (out of 154)	0,05438032
mTOR signaling pathway	5 (out of 181)	0,09609386

Gene Ontology (GoSeq)				
GO term	**Category**	**Ontology**	**Number of DR genes**	**p-adj**
hydrolase activity	GO:0016787	MF	29 (out of 1268)	1,34E-07
peptidase activity	GO:0008233	MF	14 (out of 435)	0,00012964
proteolysis	GO:0006508	BP	18 (out of 752)	0,00012964
lysosome	GO:0005764	CC	7 (out of 74)	0,00012964
cysteine-type peptidase activity	GO:0008234	MF	9 (out of 147)	0,00012964
hydrolase activity, acting on glycosyl bonds	GO:0016798	MF	6 (out of 74)	0,004329959
metabolic process	GO:0008152	BP	6 (out of 82)	0,007120488
carbohydrate metabolic process	GO:0005975	BP	8 (out of 208)	0,013229959
lysosomal membrane	GO:0005765	CC	4 (out of 46)	0,078774283

Supplementary table S4. KEGG pathway and Gene Ontology (GoSeq) analysis